JOURNAL OF THE ROYAL SOCIETY Interface

Biomechanics of the cardiovascular system: the aorta as an illustratory example

Ghassan S Kassab

J. R. Soc. Interface 2006 **3**, 719-740
doi: 10.1098/rsif.2006.0138

JOURNAL OF THE ROYAL SOCIETY Interface

J. R. Soc. Interface (2006) **3**, 719–740
doi:10.1098/rsif.2006.0138
Published online 5 July 2006

REVIEW

Biomechanics of the cardiovascular system: the aorta as an illustratory example

Ghassan S. Kassab*

Departments of Biomedical Engineering, Surgery, Cellular and Integrative Physiology, Indiana University Purdue University Indianapolis, IN 46202, USA

Biomechanics relates the function of a physiological system to its structure. The objective of biomechanics is to deduce the function of a system from its geometry, material properties and boundary conditions based on the balance laws of mechanics (e.g. conservation of mass, momentum and energy). In the present review, we shall outline the general approach of biomechanics. As this is an enormously broad field, we shall consider a detailed biomechanical analysis of the aorta as an illustration. Specifically, we will consider the geometry and material properties of the aorta in conjunction with appropriate boundary conditions to formulate and solve several well-posed boundary value problems. Among other issues, we shall consider the effect of longitudinal pre-stretch and surrounding tissue on the mechanical status of the vessel wall. The solutions of the boundary value problems predict the presence of mechanical homeostasis in the vessel wall. The implications of mechanical homeostasis on growth, remodelling and postnatal development of the aorta are considered.

Keywords: structure; function; material properties; boundary value problem; homeostasis remodelling

1. INTRODUCTION

1.1. CV system

The cardio-vascular (CV) system generally consists of heart (cardio) and blood vessels (vascular). Specifically, the CV system can be viewed as the pulmonary circulation (composed of the right heart and the lungs) and the systemic circulation in which the left heart supplies blood to the systemic organs (heart muscle, brain, skeletal muscle, bone, gastrointestinal system, spleen, liver, kidney, skin and others). The pulmonary and systemic circulations are arranged in series and hence the right and left heart chambers must pump identical volumetric flow rate in health.

The primary function of the CV system is to circulate the blood through the capillaries to within diffusion distances (less than or equal to 10 μm) of every tissue parenchyma. The blood serves as the vehicle for delivery and removal of nutrients and waste products, respectively, and the vessels serve as the highways. The blood vessels are not merely highways or pipe channels, however, as they have a passive capacitance function that maintains the blood pressure in diastole as well as an active auto-regulatory control that allows the organ to respond to local demands.

The discovery of blood circulation was made nearly four centuries ago in 1615 by William Harvey well before the discovery of capillary vessels by Marcello Malpighi in 1661 (Young 1930). Hence, the existence of capillary vessels was a theoretical prerequisite for Harvey's theory of circulation. With the discovery of capillary vessels to complete the vascular circuit and the obvious mechanical nature of the circulation, the marriage of CV physiology and mechanics was consummated; i.e. CV biomechanics.

1.2. Biomechanics

1.2.1. Definition and scope. Biomechanics is broadly defined as mechanics applied to biology. Mechanics constitutes the study of motion and associated forces while biology is the study of life. Hence, biomechanics is the interface of two large fields which includes such areas as gait analysis, rehabilitation, sports performance, flight of birds, swimming of sperm, birth labour, surgical devices, biomaterials, plant growth, prosthesis design and invertebrate mechanics to name just a few. In the present context, we shall focus the scope of biomechanics to continuum mechanics as applied to physiology. Physiology is the study of the normal function of living systems, which was originally concerned with the function of the Earth (Singer 1959). The physiologist generally seeks to understand the relationship between structure and function. Biomechanics provides the physical and analytical tools to connect structure and function with the major objective

*gkassab@iupui.edu

Received 13 April 2006
Accepted 31 May 2006

to understand problems in physiology with mathematical accuracy. In the context of vascular mechanics, the major objective is to accurately predict the mechanical environment of the cells within the arterial wall, which is the major determinant of cellular homeostasis.

Continuum mechanics is concerned with the mechanical behaviour of fluids and solids on a continuum scale; i.e. their physical properties (mass, momentum, energy, etc.) can be defined by continuous functions. In the continuum model, the scale of interest is large compared with the characteristic dimension of the discrete constituents; e.g. tissues in an organ, cells in a tissue, proteins in a cell, etc. The key concepts of continuum mechanics are stress (force/area), strain (a dimensional change) and rate-of-deformation. The physical laws of continuum mechanics include conservation of mass, momentum and energy. The material properties of a continuum are mathematically described by the constitutive equation that relate stress to strain and strain rate. The constitutive relation is generally determined by experiment under theoretical constraints including thermodynamics and other physical conditions.

Tensors are the language of continuum mechanics. Both stress and strain are tensor quantities represented by a 3×3 matrix with nine components in three-dimensional space. Since both stress and strain are symmetric tensors in the absence of external moments, the number of independent components reduces to six. The rows correspond to the direction of outer normal to a surface whereas the columns correspond to the direction of force. For a cylinder, the three directions are circumferential, longitudinal and radial.

1.2.2. Approach. As proposed by Fung (1993), there are four basic prerequisites to the solution of any problem in biomechanics: (i) identification of geometry or structure of the system; (ii) determination of the materials of the system and delineation of their mechanical properties; (iii) the basic laws governing the system; and (iv) the initial and boundary conditions. The first includes anatomical, morphological, histological and micro-structural studies. The second involves the study of chemistry, mechanical testing and constitutive formulation. The third issue depends on the number of assumptions invoked. The ideal approach is to minimize the number of ad hoc assumptions and to allow only the most basic principles as axioms: Newton's law of motion, the balance laws of mass, momentum, and energy; the second law of thermodynamics and so on. The final requirement of initial and boundary conditions depends on the starting point and the neighbourhood of the specific problem at hand, respectively. Collectively this approach leads to what mathematicians term well-posed boundary value problems (BVPs). In this way, biomechanics provides a mathematical framework for integration of structure and material properties to predict function.

1.3. Scope of the present review

It is obvious that CV biomechanics is a very broad discipline that includes the heart, blood vessels, blood cells, micro-circulation, etc. Indeed, a PubMed Search under Cardiovascular Biomechanics found 30 114 reports. Even for Biomechanics and Aorta, PubMed lists 4426 entries. We refer the reader to several excellent reviews on vascular mechanics in the last decade (e.g. Humphrey 1995; Fung 1996; Holzapfel & Weizsacker 1998; Vito & Dixon, 2003) and specifically on the aorta (e.g. O'Rourke 1994; Belz 1995).

In the present review, we shall focus Fung's biomechanics approach on the aorta and demonstrate some of the rewards reaped through this approach. We will consider the geometry and material properties of the aorta to formulate well-posed BVPs. Finally, we will discuss the physiological implications of the biomechanical analysis. Specifically, we will consider the biomechanical homeostasis of the vessel wall and its implications on growth, remodelling and postnatal development.

2. PHYSIOLOGY OF AORTA

The aorta is the most proximal artery connected directly to the heart and acts both as a conduit and an elastic chamber. In its latter role, the aorta's elasticity serves to convert the heart's pulsatile flow to nearly steady flow in peripheral vessels. Stephen Hales (1733) reported his observations that the aorta expands to accommodate a large fraction of the stroke volume. Hales reasoned that the aorta serves as an elastic reservoir, which distends with blood during the heart's contraction and discharges blood through the peripheral resistance by elastic recoil while the heart refills. His explanation accounts for the smoothing action of the aorta in converting the pulsatile flow of the heart to smooth flow in blood vessels. An analogy was made with a hand-pump fire engine which smoothes a pump's pulsatile flow of water. In 1899, Otto Frank used this analogy to formulate the well known Windkessel theory.

This review emphasizes data from the author's laboratory which are primarily from two animal models: mice and pigs (Guo *et al.* 2002, 2005; Guo & Kassab 2003, 2004; Huang *et al.* 2006). It may be appropriate to say a few words about the choice of animal models. The inbred strains of mice are being used with increasing frequency in many experimental CV studies (Hanahan 1990; Faraci & Sigmund 1999) because knockout studies have led to sub-strains that are predisposed to hypertension, diabetes and hypercholestermia, all of which are important risk factors for CV disease (Dunn 1965; Russell & Meier 1966; Russell 1972; Plump *et al.* 1992; Fyfe *et al.* 1994). Each strain has a heritable life-span (Russell 1966; Storer 1966; Festing & Blackmore 1971; Grahn 1972; Russell 1972) and a heritable characteristic pattern of disease (Dunn 1965; Russell & Meier 1966; Russell 1972; Sucov 1998). The focus on the mouse model is necessary to advance the phenotypic characterization of the mouse aorta in connection with genotypic manipulations.

The swine model is extremely popular in CV research because of the anatomical and hemodynamic similarities to humans (Hughes 1986; Hughes *et al.* 2003). In addition to similarities in hemodynamics (blood pressure, heart rate, cardiac output (CO), etc.), the extent of collateral vessels and the size distribution of the coronary arteries in the heart are also very comparable to man (White & Bloor 1981; Sack 1982). Hence, the swine aorta model is extremely important to advance our knowledge of human CV physiology and it is imperative for clinical (aortic aneurysm, dissection, etc.) and translational research (e.g. endovascular aneurysm repair). In addition to the mouse and pig models, there is enormous literature on the biomechanics of aorta in rat (Safar *et al.* 1998), rabbit (Chien 1978), dog (Ito *et al.* 1977), human (O'Rourke & Nichols 2005) and other species.

3. STRUCTURE OF AORTA

3.1. Introduction

The prescription of geometry or morphometry (measurement of form or shape) is necessary for the formulation of any BVP. Since BVP has values assigned on the physical boundary of the domain in which the problem is specified, the importance of geometry or form is obvious. Specifically, there are several reasons for specifications of geometry: (i) a mathematical model of the aorta must obey geometric similarity, which requires knowledge of the diameter and lengths of every segment of aorta; (ii) a mathematical analysis of aorta must also obey the rule of dynamic similarity which reduces to the simulation of two dimensionless parameters, the Reynolds number, N_R ($N_R = \rho UD/\mu$ where U is the mean flow velocity, D is the lumen diameter of vessel, and ρ and μ are the density and viscosity of blood, respectively); and Womersley number, N_W ($N_W = D/2(\rho\omega/\mu)^{1/2}$, where ω is the circular frequency of pulsatile flow); (iii) for a steady laminar flow, Poiseuille's formula states that the flow rate (volume/time) is directly proportional to the product of the fourth power of the diameter and the pressure drop and is inversely proportional to the first power of the vessel length, (iv) in an unsteady flow, the characteristic impedance is the ratio $\rho c/A$ where ρ is the density of blood, c is the speed of flexural waves in the blood vessel and A is the cross-sectional area (CSA; proportional to the square of diameter) of the vessel; and (v) the mean circumferential Cauchy stress, σ (force per deformed area), in the vessel wall is given by $\sigma = PD/2h$, where P is the blood pressure and h is the wall thickness. Hence, it is clear that the geometry of the aorta (e.g. diameter, length, wall thickness and curvature) must be quantified for a realistic biomechanical analysis of aortic function.

3.2. Imaging of geometry

Since a detailed biomechanical analysis requires data on the geometry of an organ (e.g. the shape of the heart and the size of the blood vessels), developments in biomechanics overlap with advances in anatomy and imaging. Structural imaging is necessary for quantifying organs, tissues, cellular and molecular structures, which serve as a basis for the construction of biomechanical and integrative models. Imaging modalities include magnetic resonance imaging (MRI), computerized tomography (CT), positron emission tomography (PET) and ultrasound (US) at the organ level, micro-CT and optical coherence tomography at the tissue level, confocal and interference microscopy, multi-photon microscopy (MPM) and electron tomography (ET) at the cellular level and X-ray crystallography at the molecular level. Some of these modalities have been used for imaging of aorta (e.g. ET, Thompson & Stanford 1994; PET, Alavi *et al.* 2002; US, Long *et al.* 2004; CT, Kang & Spain 2005; MRI, McGuigan *et al.* 2005).

3.3. Longitudinal geometry of aorta

Recently, we used US to measure the *in vivo* geometry of the mouse aorta as shown in figure 1 (Guo *et al.* 2002). A cast was used to validate the US diameter measurements and to reconstruct the morphometry of the entire length of the aorta from the aortic valve to the common iliac bifurcation as illustrated in figure 2. The coordinates x and a are referred to as the fractional longitudinal position (FLP) in the loaded (physiological pressure) and no-load (zero transmural pressure) states, respectively (with $x=0$ at the aortic valve and $x=1$ at the point of common iliac bifurcation). Table 1 shows the relationship between the various anatomical bifurcations (thoracic, abdominal, renal, etc.) and the FLP. These data serve to quantify the anatomy of the aorta relative to anatomical bifurcations and are essential for comparison of the length-normalized aorta of various species.

The longitudinal variation of the inner and outer diameters of the mouse aorta at physiological pressure (100 mmHg) is shown in figure 3*a*. It should be noted that the nearly linear taper geometry is only an approximation. In reality, the diameter changes take place only at the branching points; i.e. the vessel segments are cylindrical between bifurcation points. This observation was first made by Sobin and applies to many vascular and botanical trees (Sobin & Chen 1997). Sobin's observation postulates that the apparent taper of a large artery is due to side branches. Hence, the taper is only an approximation to what is actually a stair-case change in diameter.

The wall thickness at the loaded state was computed as the difference between the outer and inner radius of the vessel as depicted in figure 3*b*. The wall thickness shows a linear variation whose empirical constants are summarized in the figure legend. The radius of curvature of the aortic arch is shown in figure 3*c*. The curvature, which is the inverse of radius of curvature, is greatest at FLP of 0.11. An analysis of stress distribution in the aortic arch must take into account the curvature since a larger curvature leads to a greater non-uniformity in the circumferential transmural stress distribution. The mouse aortic arch data is similar to that found in the rat (Liu & Fung 1988).

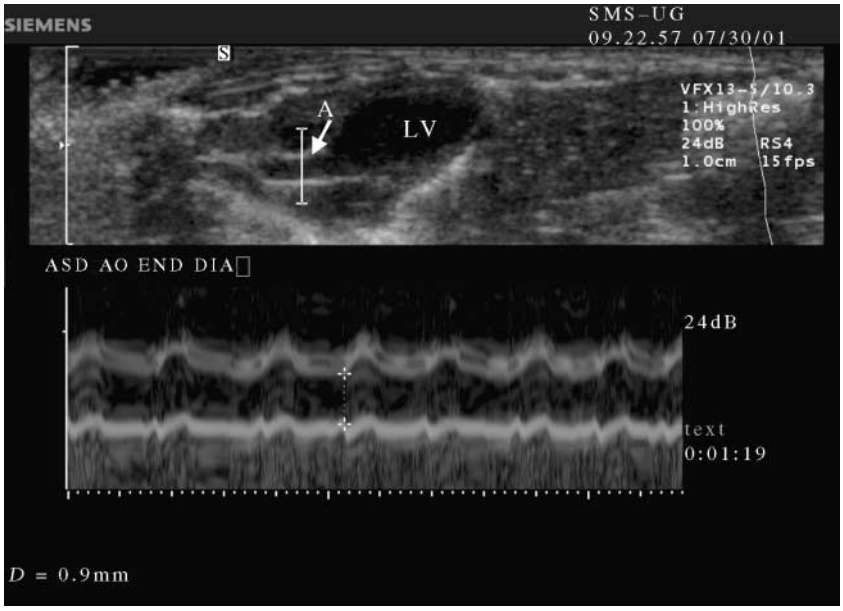

Figure 1. An ultrasound image of the ascending aorta. M-mode (lower image) was applied vertically to the aorta (cursor at ascending aorta in upper image) to measure end diastolic diameter. LV and Ao denoted left ventricle and ascending aorta, respectively. (Reproduced with permission from Guo *et al.* (2002).)

The variation in the wall area was nonlinear and can be described by a higher order polynomial (Guo *et al.* 2002). Han & Fung (1995) have previously determined the longitudinal variation of the wall CSA of the dog and pig aorta. They found species differences in the thoracic region. The longitudinal variation of the wall area of the pig and mouse aortas is very similar. With the establishment of a geometric model of mouse aorta, a biofluid or biosolid mechanical analysis can be advanced.

3.4. Wall micro-structure

Arteries are generally subdivided into two types: (i) elastic (e.g. aorta, carotids and pulmonary arterial vessels) and (ii) muscular (e.g. coronary, femoral and cerebral arteries; Burkitt *et al.* 1993). The wall structure of both types of arteries consists of intima, media and adventitia. The *intima* layer consists of relatively acellular fibrous tissue and ground substance covered by a monolayer of endothelial cells. The *media* is composed of multiple layers of smooth muscle cells separated by collagen, ground substance and elastic fibres. There are numerous elastic laminae and smooth muscle cells in the aortic media. The *adventitia* has bundles of collagen and loose bands of elastic tissue. The intima and media, and media and adventitia are separated by internal and external elastic laminae, respectively. The aorta has a vasa vasorum which is located in the adventitial layer and penetrates to varying depths into the outermost portion of the medial layer.

3.4.1. Early work. The mechanical properties of blood vessels are derived from collagen and elastin fibres, smooth muscle cells and ground substances. The idea of relating the macroscopic mechanical properties of arteries to the micro-structure of the wall was first

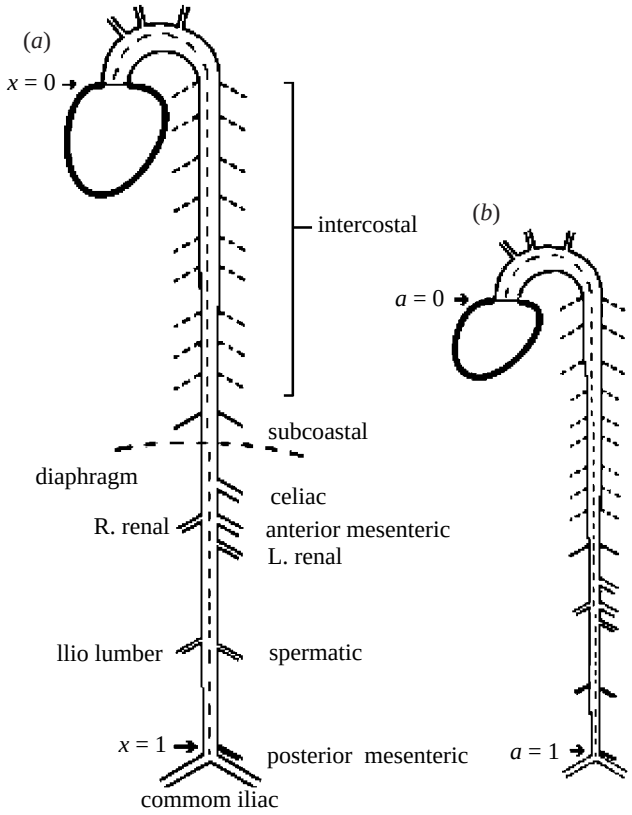

Figure 2. A schematic of the aorta in the (*a*) loaded and (*b*) no-load state. The coordinate systems x and a are shown for the loaded and no-load states, respectively. (Modified with permission from Guo *et al.* (2002).)

demonstrated by Alan Burton and colleagues. Roach & Burton (1959) studied arteries by differential digestion of elastin or collagen in the artery and measured the resulting mechanical changes of the artery after digestion. Based on this idea, Oka (1972) formulated a theoretical analysis of arterial wall which resulted in several important studies by Oka & Azuma (1970),

Table 1. The fractional longitudinal position (FLP) of the aortic bifurcations.

FLP ± s.d.	aortic branch
0	aortic semilunar valve
0.041 ± 0.0098	innominate artery
0.075 ± 0.011	left common carotid artery
0.12 ± 0.011	left subclavian artery
0.20 ± 0.013	1st pair of intercostals artery
0.24 ± 0.014	2nd pair of intercostals artery
0.29 ± 0.0066	3rd pair of intercostals artery
0.34 ± 0.0087	4th pair of intercostals artery
0.38 ± 0.0080	5th pair of intercostals artery
0.42 ± 0.0064	6th pair of intercostals artery
0.47 ± 0.0087	7th pair of intercostals artery
0.51 ± 0.0096	8th pair of intercostals artery
0.55 ± 0.012	9th pair of intercostals artery
0.61 ± 0.012	subcostal artery
0.69 ± 0.013	celiac artery
0.73 ± 0.012	right renal artery
0.78 ± 0.014	left renal artery
0.86 ± 0.015	illio-lumbar artery
1	common iliac artery

Azuma & Oka (1971) and Azuma & Hasagawa (1971). Azuma & Hasegawa discussed the rheological properties of arteries and veins in terms of the networks of collagen, elastin and smooth muscles in the wall. Generally, the attempts to determine the geometry (width, length, curvature, orientation) of the collagen and elastin fibres in the artery have not been fruitful because the mat of fibres is so dense and closely knit that it is difficult to make the needed measurements.

3.4.2. Micro-structure-based constitutive models. In relating the micro-structure and overall constitutive response of arteries, researchers have proposed several constitutive models. Decraemer *et al.* (1980) proposed a parallel wavy fibres model for soft biological tissues in uniaxial tension. Lanir (1983) further developed a general multi-axial theory for the constitutive relations in fibrous connective tissues on the basis of micro-structural and thermodynamics consideration. Based on the entropy evolution in rubber elasticity (Treloar 1975), Arruda & Boyce (2004) and Bischoff *et al.* (2002) developed a hyperelastic constitutive model. Their model has been employed in biological simulations, including recent work on arterial hypertension. There are also general theories for woven fabric (Nayfeh & Kress 1997) and random polymer or spring networks (Idiris *et al.* 2000; Rubinstein & Panyukov 2002; DiDonna & Lubensky 2005). The previous micro-structure-based constitutive model, however, have not been well rooted in quantitative data on the vascular micro-structure. Recently, Holzapfel & Gasser (2000) proposed a constitutive framework for arterial wall mechanics by treating the vessel wall as a two-layer fibre-reinforced composite with the fibres corresponding to the collagenous component of the arteries. In their model, the fibres are symmetrically disposed with respect to the cylinder axis resulting in an orthotropic constitutive law for each layer. Although promising, this model has not yet been micro-structurally validated.

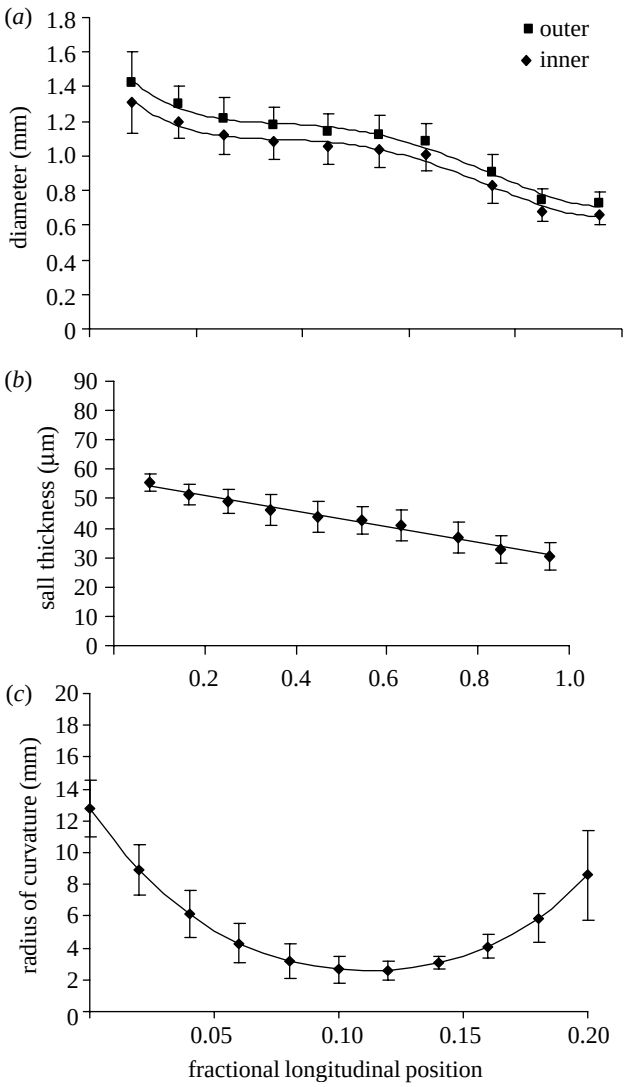

Figure 3. Morphometry of the mouse aorta in the loaded state (100 mmHg). (*a*) Inner and outer diameters, D_i and D_o, respectively as a function of fractional longitudinal position, FLP. Least-square curves are of fourth-order polynomial ($D_o = 9.1\text{FLP}^4 - 20.2\text{FLP}^3 + 14.6\text{FLP}^2 - 4.5\text{FLP} + 1.7$, $R^2 = 0.989$; $D_i = 8.9\text{FLP}^4 - 19.7\text{FLP}^3 + 14.3\text{FLP}^2 - 4.4\text{FLP} + 1.6$, $R^2 = 0.989$). (*b*) WT, Wall thickness. A least-square fit is used to fit the wall thickness data as $\text{WT} = -26.8\text{FLP} + 56.5$ ($R^2 = 0.988$). (*c*) RC, Radius of curvature, of the centreline can be described by a least-square fit as $\text{RC} = 805\text{FLP}^2 - 180\text{FLP} + 12.4$, $R^2 = 0.995$. (Reproduced with permission from Guo *et al.* (2002).)

3.4.3. Recent developments. Recently, a non-destructive method has been developed to provide quantitative data on the three-dimensioanl structure of collagen and elastin. Tromberg and colleagues have recently demonstrated the co-registration of two-photon excited fluorescence (TPEF) and second-harmonic generation (SHG) in unfixed, unstained tissue in reflection geometry (Zoumi *et al.* 2002, 2004). Spectral measurements were employed to determine the origin of the image-forming signal from structural proteins in arteries (Zoumi *et al.* 2004). At shorter excitation wavelengths the signal

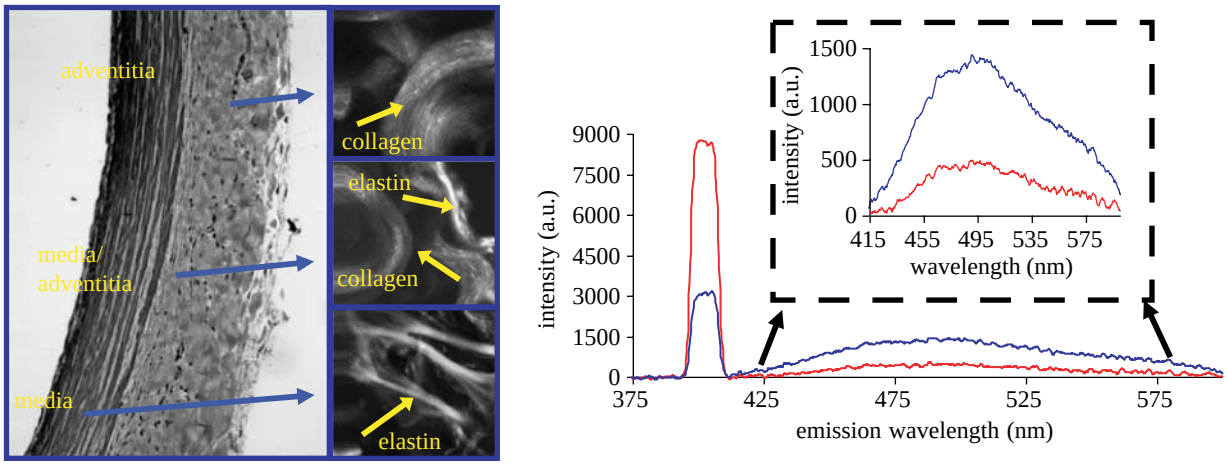

Figure 4. Histology and multi-photon microscopy of the rabbit aortic wall. (*a*) Two-dimensional image sections of the rabbit aorta recorded at different x- positions for $\lambda_{ex}=800$ nm and $P=60.2$ mW for the adventitia, the adventitia-media border and the media. (*b*) Emission spectra corresponding to the adventitia-media border and the media are shown. The boxed region is a zoomed in version of the lower plot. Photo reproduced courtesy of Dr Bruce Tromberg.

emitted from collagen is a combination of SHG and TPEF whereas at longer excitation wavelengths, the collagen emission is exclusively due to SHG. The signal from elastin is solely due to TPEF. The spectrally distinct origin of signals from the different arterial components may allow the selective visualization of the structural and functional modifications of collagen and elastin during various physiological and pathophysiologic conditions. Using SHG and TPEF in combination provides complementary information that allows non-invasive, spatially localized characterization of arterial tissue.

We recently performed histochemical analysis of the aorta to facilitate mapping of the different layers in the vessel wall. Figure 4 shows SHG/TPEF images of the aortic wall obtained from the adventitia, the adventitia-media border and the media, respectively, for $\lambda_{ex}=800$ nm. The images are consistent with the histology, displaying sheets of collagenous fibres oriented in multiple directions in the adventitia and mainly elastic fibres in the media.

A major advantage of this approach for studying arterial tissue is that it relies exclusively on endogenous signals and does not require exogenous probes, which can change the biological state of the tissue. Due to the near-infrared wavelengths used, greater penetration depths can be achieved. Furthermore, photo-damage and photo-bleaching are largely eliminated, thus rendering combined SHG/TPEF the technique of choice for intravital imaging. Finally, this method allows simultaneous mechanical testing and visualization of the micro-structural components in the same specimen. Current efforts are underway to quantify the three-dimensional geometry of elastin and collagen fibres to provide a micro-structural model to predict the macro-mechanical properties of vessel wall.

4. MATERIAL PROPERTIES OF AORTA

4.1. Introduction

Biological tissues are subject to the same balance laws of conservation of mass, momentum and energy. What distinguish biological tissues from inanimate materials are their unique constitutive equations. The literature on the material properties (e.g. stiffness) of the aorta is enormous (Fung 1990, 1993; Nichols & O'Rourke 1990). One of the reasons for the great interest stems from the observation that increased stiffness of large elastic arteries represents an early risk factor for CV diseases (Arnett *et al.* 1991; Hodes *et al.* 1995). Specifically, increased aortic stiffness is associated with atherosclerosis (Dart *et al.* 1991), aging (Russell & Meier 1966; Avolio *et al.* 1983; Gillensen *et al.* 1995), heart failure (Khan *et al.* 1999) and various risk factors such as hypertension (Dzau & Safar 1988; Heints *et al.* 1993), diabetes (Liu & Fung 1992; Airaksinen *et al.* 1993; Salomma *et al.* 1995), hyperlipidemia (Lehmann *et al.* 1992) and smoking (Liu & Fung 1993; Stefanadis *et al.* 1997). Furthermore, arterial stiffness has also been shown to be an independent risk factor for CV events such as primary coronary events, stroke and mortality (Boutouyrie *et al.* 2002; Laurent *et al.* 2003). Therefore, the assessment of aortic mechanical properties is particularly important in understanding the mechanisms of CV disease.

4.2. Pressure–diameter–length relation

The pressure–diameter relation has been very popular in CV physiology because it plays an important role in the pressure–flow relationship of blood flow through the vessel and hence the organ. In fact, the compliance of the vasculature (slope of the pressure–diameter relation) is an important determinant of the non-linearity of the pressure–flow relationship (Fung 1990; Kassab 2001). Furthermore, the pressure–diameter–length relation can be transformed into a biaxial (circumferential and longitudinal) stress–strain relation where the mean circumferential Cauchy stress is computed from pressure, diameter and wall thickness as per Laplace's equation and strain is computed from circumference (or diameter) measurements in reference to the zero-stress state (Guo & Kassab 2003). The major advantage of the pressure–diameter

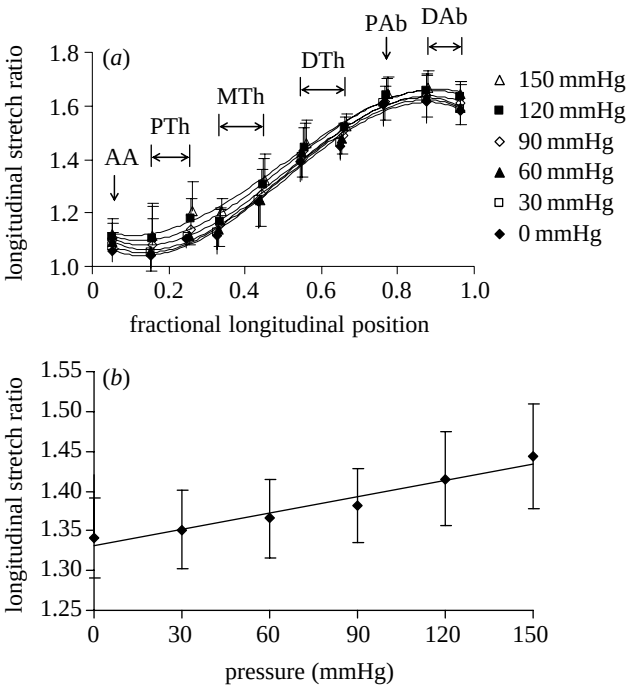

Figure 5. (*a*) The variation of the local longitudinal stretch ratio with the location along the long axis of the aorta (FLP, fractional longitudinal position) at the different pressures. AA, PTh, MTh, DTh, PAb and DAb represent ascending aorta, proximal thoracic, middle thoracic, distal thoracic, proximal abdominal and distal abdominal, respectively. (*b*) The variation of the global longitudinal stretch ratio of aorta (λ_z^g) with the pressures (P). The solid line is a polynomial regression curve of the form $\lambda_z^g = 6.82 \times 10^{-4} P + 1.33$, $R^2 = 0.953$. (Reproduced with permission from Guo & Kassab (2003).)

protocol is that it preserves the coupled nature of mechanical loading unlike the uniaxial strip experiments.

4.2.1. Longitudinal stretch ratio. The pressure–diameter–length relation was determined in the aorta of mice *in situ* (Guo & Kassab 2003). The *in situ* state preserves the effect of surrounding tissue unlike the *ex-vivo* experiment. The longitudinal stretch ratio of the aorta *in situ* was obtained as the ratio of the segmental length at various pressures relative to the zero-stress state. The lengths of the mouse aorta (body weight of 25.3 ± 1.3 g), from the aortic valve to the common iliac bifurcation, were 41.4 ± 2.4 and 29.5 ± 1.7 mm in the loaded and no-load states, respectively. Hence, the average longitudinal stretch ratio is approximately 1.4.

Figure 5*a* shows the variation of the local longitudinal stretch ratio along the length of the mouse aorta at different distension pressures. Figure 5*a* shows that the longitudinal stretch ratio increases along the length of the aorta (larger near the common illiac bifurcation) similar to canine and porcine aortas (Han & Fung 1995) and increases with pressure at any longitudinal position. The former observation is very pronounced where the stretch ratio is near one at the ascending aorta and 1.6 near the common illiac bifurcation. Consequently, when the vessel is excised the various

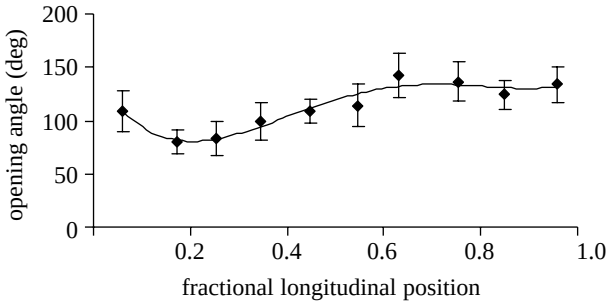

Figure 6. The variation of opening angle (θ) with the position along the aorta (FLP, fractional longitudinal position). (Reproduced with permission from Guo *et al.* (2002).)

regions will shorten according to figure 5*a* where the abdominal aorta shortens the most. Although the latter shows a smaller change with pressure, it deserves mention as most *in vitro* studies maintain constant longitudinal stretch ratio during inflation which is not physiological.

The global stretch ratio is measured as the ratio of the total length of the aorta at a given pressure to the *in vitro* length at no-load state (approximately equivalent to zero-stress). Figure 5*b* shows the variation of the global longitudinal stretch ratio of mouse aorta as a function of pressure. As the pressure increases, the global longitudinal stretch ratio shows a significant increase, which suggest elongation of aorta and possible increase in curvature. This may be important in hypertension as increase of curvature and bending may be atherogenic.

4.2.2. Zero-stress state. It has been more than 20 years now since Fung (1984) and Vaishnav & Vossoughi (1983) independently showed that the zero stress state of a blood vessel is an open sector. This was a critical observation for vessel mechanics since all computations of stress and strain must be referred to the zero stress state that had erroneously been assumed to be the no-load configuration (i.e. a tube). Since then, numerous papers have been written on the subject as detailed in Fung (1990) and more recently reviewed by Rachev & Greenwald (2003).

The open sector in the zero-stress state has been characterized by the opening angle that is defined as the angle subtended by two radii connecting the midpoint of the inner wall to the ends of the open segment as shown in figure 10. The longitudinal variation of the opening angle in the mouse is shown in figure 6. The longitudinal variation of the opening angle has been previously documented in the rat and pig aortas (Liu & Fung 1988; Han & Fung 1991). Both pig and rat aortas have a mean opening angle of about 130° in the ascending aorta region similar to that found in the mouse (Guo *et al.* 2002; Guo & Kassab 2003). The species differences become evident, however, in the thoracic aorta region. It appears that the aortic longitudinal variation of opening angle in the mouse model is more similar to the pig than to the rat. Furthermore, the variation of opening angle in the mouse aorta was similar to post-mortem data of human aorta that did not show a minimum value in the middle

portion of the aorta (Saini *et al.* 1995). Direct numerical comparison of opening angles is difficult, however, since the human aorta data were obtained 24 h after death.

4.2.3. Stress and strain. For large deformation of a cylindrical vessel, the circumferential Green–Lagrange strain E_c ($E_c = (1/2)(\lambda_c^2 - 1)$; $\lambda_c = C/C_{zs}$ where C and C_{zs} represent the circumferences at loaded and zero-stress state) is an appropriate measure. For anisotropic materials, the stress–strain relation should be established between the 2nd Piola–Kirchhoff (P–K) stress and the Green–Lagrangian strain (Atluri 1984). The circumferential 2nd Piola–Kirchhoff (P–K), S_c, can be easily computed from the Cauchy stress, σ_c ($\sigma_c = Pr/h$ as given by Laplace's equation; P, r and h represent the blood pressure, inner radius and wall thickness, respectively) as $S_c = \sigma_c/\lambda_c^2$. The Cauchy (true) stress is the force per *deformed* area whereas the 2nd Piola–Kirchhoff stress is the force per *undeformed* area.

The relation between average circumferential and longitudinal Green strains and 2nd Piola–Kirchhoff stresses for the middle thoracic and abdominal aorta in the pressure range of 30–210 mmHg are shown in figure 7*a*. It can be seen that the relationship is linear up to 120 mmHg (i.e. physiological range) beyond which it becomes nonlinear. It is also interesting to note that the relationship in the two regions is essentially the same below 120 mmHg. Above this pressure the abdominal aorta attains larger stresses and strains. This observation may be due to the fact that the abdominal aorta has fewer bifurcation constraints and is less tethered by the surrounding tissue. This observation underscores an interesting possible correlation between higher stresses and strains with the predisposition of disease in the abdominal aorta in hypertension (DeBakey *et al.* 1985). Interestingly, the porcine abdominal aorta reveals higher opening angle, strain and stress as compared to the thoracic aorta under normotensive conditions (Guo & Kassab 2004).

Figure 7*b* shows the circumferential stress–strain relationship for various segments of the aorta in the 30–120 mmHg pressure range while figure 7*c* shows the corresponding data for the longitudinal stress–strain relation. The observed linearity of mechanical properties in the *in vivo* range (30–120 mmHg) along the length of the aorta will simplify future mechanical modelling of the mouse CV system (Guo & Kassab 2003).

4.2.4. Constitutive equation. The constitutive equation of the blood vessel wall was a much debated subject in earlier years (see review in Fung 1993). Eventually, the following observation by Fung (1993) was generally accepted: soft tissues have a special kind of viscoelasticity where the percentage loss of energy by hysteresis per cycle in a cyclic loading and unloading process is only a few percent, and this percentage does not vary more than a factor of two over a frequency range of five orders of magnitude. However, at any particular frequency, it is not easy to predict the exact value of the loss per cycle. Fung (1993) and others showed that this is consistent with a model of viscoelasticity with a

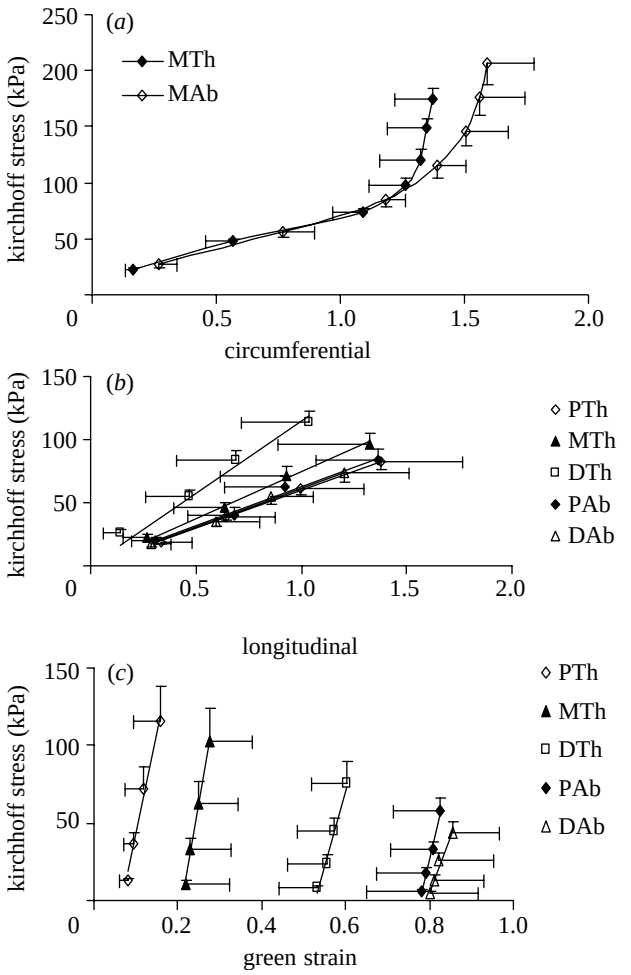

Figure 7. (*a*) The circumferential second Piola–Kirchhoff stress/Lagrange–Green strain relation for the middle thoracic (MTh) and abdominal (MAb) aorta in the 30–210 mmHg pressure range. The (*b*) circumferential (*c*) and longitudinal stress–strain relationship in the pressure range of 30–120 mmHg. PTh, MTh, DTh, PAb and DAb denote proximal thoracic, middle thoracic, proximal thoracic, proximal abdominal and distal abdominal aorta, respectively. (Reproduced with permission from Guo & Kassab (2003).)

continuous relaxation spectrum. In cyclic loading and unloading the stress–strain relationship is unique in the loading stroke, and is also unique in the unloading stroke (although the two are somewhat different because of hysteresis). Fung called such a material *pseudo elastic*, a term which is now widely used. In this framework, the viscoelastic hysteresis behaviour of soft tissue can be approximated within the more tractable framework of elasticity, provided that the elastic properties are different for loading and unloading.

A well-known approach to the study of elasticity of bodies capable of finite deformation is to postulate the form of a strain energy function (SEF; Green & Adkins 1960). The SEF relates stress to strain in a hyperelastic material, which arises from changes in internal energy or entropy with loading. The partial derivatives of the SEF with respect to Green's strain components are related to the second Piola–Kirchhoff stresses. The determination of SEF is an inverse problem. A form of the SEF is assumed and based on computed values of stress and strain from loading and deformation

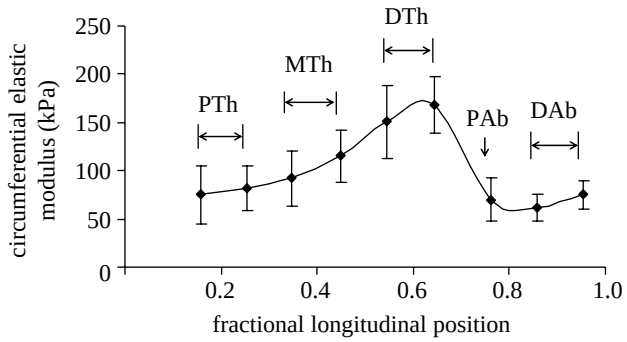

Figure 8. The variation of circumferential elastic modulus along the length of aorta. (Reproduced with permission from Guo & Kassab (2003).)

experiments, we determine the material properties that give satisfactory agreement between the theorized form and the experimental data. This procedure involves nonlinear least squares fit using the classical Marquardt-Levenberg (Marquardt 1963; Fung *et al.* 1979) or the more recent Genetic Algorithm methods (Coley 1999; Sverdlik & Lanir 2002). Genetic algorithms may be advantageous because they can determine the global minimum in highly nonlinear problems with multiple local minima (Karr *et al.* 2000; Vigdergauz 2001; Pandit *et al.* 2005). The major advantages of this approach are that it explores the solution space by testing parameter combinations simultaneously to avoid local minimum and does not require derivative information (Goldberg 1989).

Alternative analytical forms for the SEF can be found in the literature (Fung 1993; Abe *et al.* 1996), especially the polynomial form of Patel *et al.* (1973) and the logarithmic form by Hayashi (1993), but the exponential form is most widely used. Many validation experiments have been done over the years (Fung 1993). For the mouse aorta, the linear stress–strain relation reduces the form of the SEF to a simple second order polynomial (Guo & Kassab 2003).

4.2.5. Elastic moduli. The elastic modulus for a linear uniaxial stress–strain relation is defined as the slope of the curve (Young's modulus). For biaxial experiments, the elastic moduli can be generalized for an anisotropic material as given by Dobrin & Doyle (1970). The elastic moduli in the circumferential and longitudinal directions were computed for the mouse aorta (Guo & Kassab 2003). The variation of the *in situ* circumferential elastic modulus along the length of the aorta is shown in figure 8. The circumferential modulus is stiffest near the diaphragm which is consistent with the findings of Tanaka & Fung (1974) in canine aortic uniaxial strips. The mean longitudinal modulus was found to be fairly constant along the length of the mouse aorta. The longitudinal modulus was approximately two orders of magnitude larger than the circumferential modulus in the *in situ* preparation where the aorta is constrained through numerous bifurcations; and hence reflects not only the properties of the aorta but also the surrounding tissue (Guo & Kassab 2003).

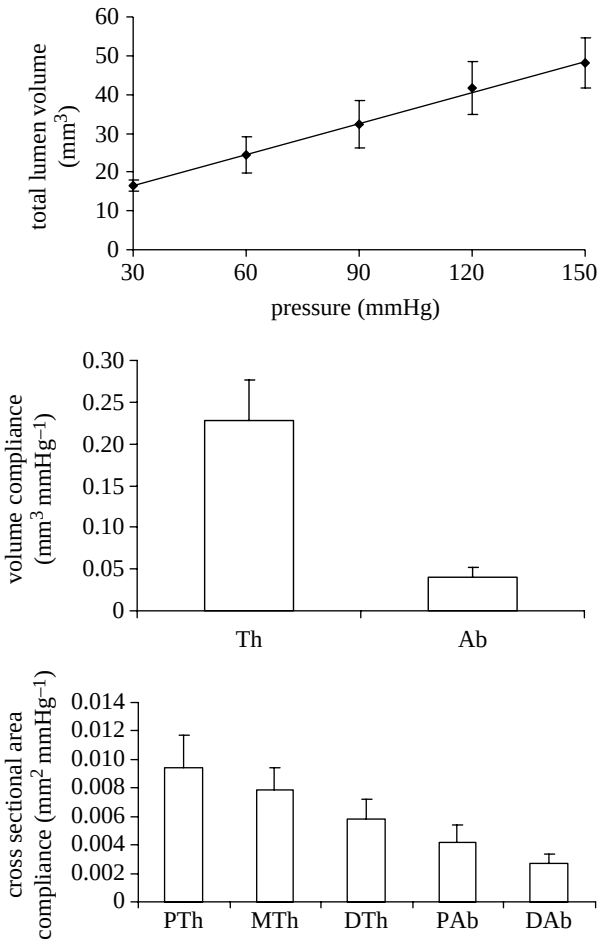

Figure 9. (*a*) The variation of total aortic lumen volume (V) with distension pressures (P). The solid line is a linear least-square fit of the form $V=2.67\times10^{-4}P+8.52\times10^{-3}$, $R^2=0.998$. (*b*) The static volume compliance ($\Delta V/\Delta P$) for the thoracic and abdominal aorta. (*c*) The cross-sectional area compliance ($\Delta\mathrm{CSA}/\Delta P$) for the various segments of aorta. The differences between aortic regions were statistically significant. (Reproduced with permission from Guo & Kassab (2003).)

4.2.6. Compliance. The variation of lumen CSA with pressure for the various segments of aorta was found to be linear. The pressure–volume relationship of the entire aorta is shown in figure 9*a* (Guo & Kassab 2003). The slope of the curve corresponds to the volume compliance ($\Delta V/\Delta P$) of the aorta which is independent of pressure in the 30–150 mmHg range. We also evaluated the volume compliance of thoracic and abdominal aorta as shown in figure 9*b*. Since the volume compliance is additive, the total volume compliance, obtained from figure 9*b*, is equal to the sum of volume compliance of thoracic and abdominal aorta. It is interesting to note that the abdominal compliance is only 15% of the thoracic compliance. Alternatively, the compliance can be expressed in terms of CSA ($\Delta\mathrm{CSA}/\Delta P$). It is much easier to measure the CSA compliance; particularily, *in vivo* (figure 9*c*). Hence, the majority of data in the literature is on the CSA compliance, which is incorrectly used interchangably with volume compliance. In any case, both CSA and volume compliance show that the proximal aorta, near the heart, is most compliant with the compliance

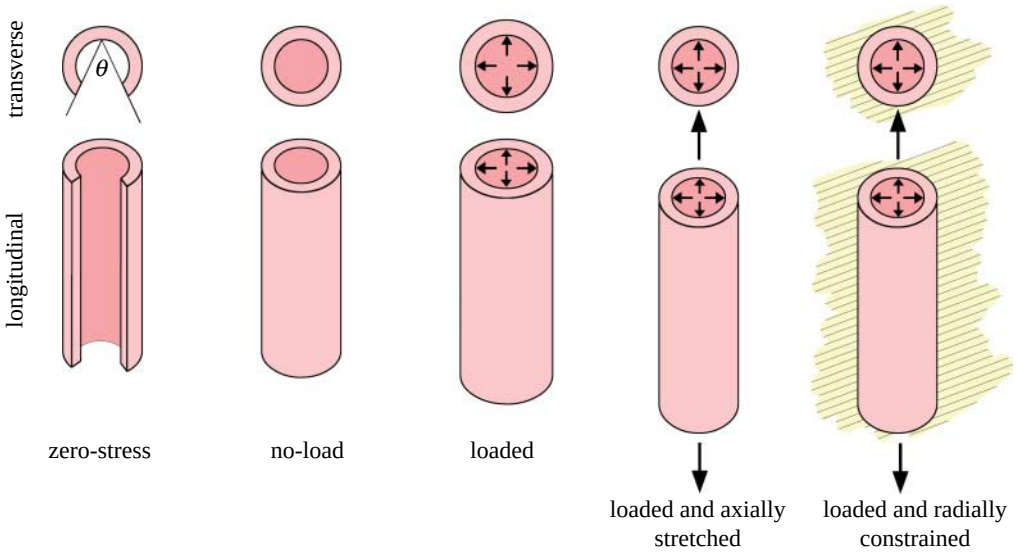

Figure 10. Schematic of the class of problems being considered. An open sector is closed followed by inflation, longitudinal extension and external radial constraint.

decreasing towards the distal aorta consistent with the Windkessel function.

Numerous estimates of compliance have been made *in vivo* based on the Windkessel model by calculation of time constant (product of total arterial resistance and compliance) of pressure decay or some modification thereof (Slordahl *et al.* 1990). Data on the compliance of pig, dog and rat have been reported as approximately 0.5 (Slordahl *et al.* 1990), 0.1 (Stergioulos *et al.* 1999) and 5×10^{-3} ml mmHg^{-1} (Levy *et al.* 1985), respectively. In the dog experiment the reported compliance corresponds to the proximal descending aorta, which accounts for 60% of the total arterial compliance. One of the limitations of the Windkessel model is that it does not account for wave reflections which should be considered when interpreting the data particularly at higher heart rates.

We can estimate the degree of accomodation that the aorta provides to each ejection of the heart. The stroke volume can be determined as the quotient of CO and heart rate while the change of volume of the aorta during each cardiac cycle can be estimated from the product of compliance and pulse pressure. For the mouse, at a CO of 12.5 ml min^{-1} and heart rate of 622 beats min^{-1}, we obtain a stroke volume of 0.02 ml (Barbee *et al.* 1992). For a pulse pressure of 25 mmHg, the computed compliance yields a change in aortic volume of 0.0067 ml. Hence the aorta can accommodate about one-third of the stroke volume. It should be noted that this is an estimate since the dynamic compliance may be somewhat different which would affect the value. Similar calculations for the pig yield a stroke volume of 20 ml assuming CO of 2 l min^{-1} and heart rate of 100 beats min^{-1}. The change in aortic volume during each cardiac cycle can be estimated as 12.5 ml assuming a pulse pressure of 25 mmHg and dynamic compliance of 0.5 ml mmHg^{-1}. Hence, the aorta accomodates about two-thirds of the blood pumped in one stroke. Incidentially, this is the same estimate made by Hales (1733) nearly three centuries ago.

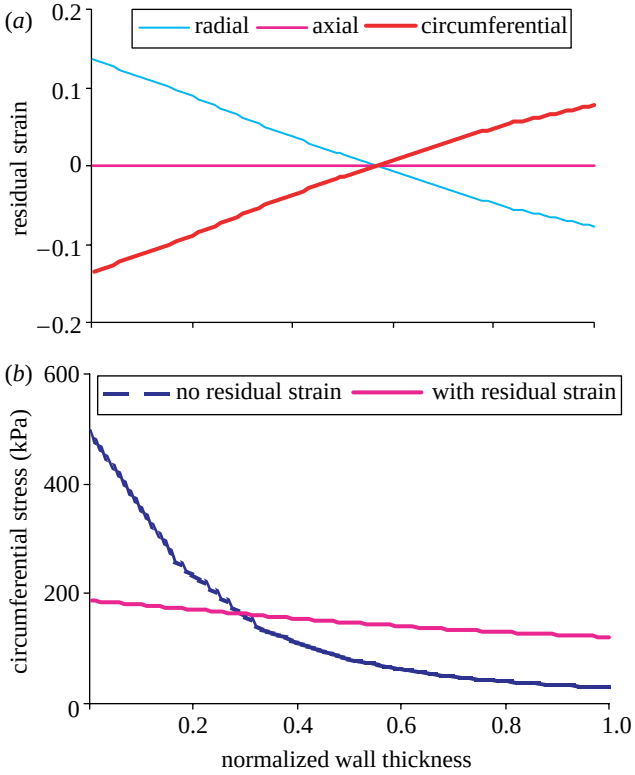

Figure 11. (*a*) Distribution of logarithmic residual strains throughout the coronary arterial wall thickness. (*b*) Circumferential Cauchy stress distributions in the coronary vessel wall at physiological conditions (for longitudinal stretch ratio of 1.4 and internal pressure of 120 mmHg). (Reproduced with permission from Zhang *et al.* (2005).)

5. BOUNDARY VALUE PROBLEMS

In the examples that follow, the BVPs are solved by applying the equation of radial equilibrium under quasi-static conditions in an axisymmetric geometry as shown in figure 10. The solutions of these BVP provide the transmural distribution of stress components. The constitutive equation and BVPs are

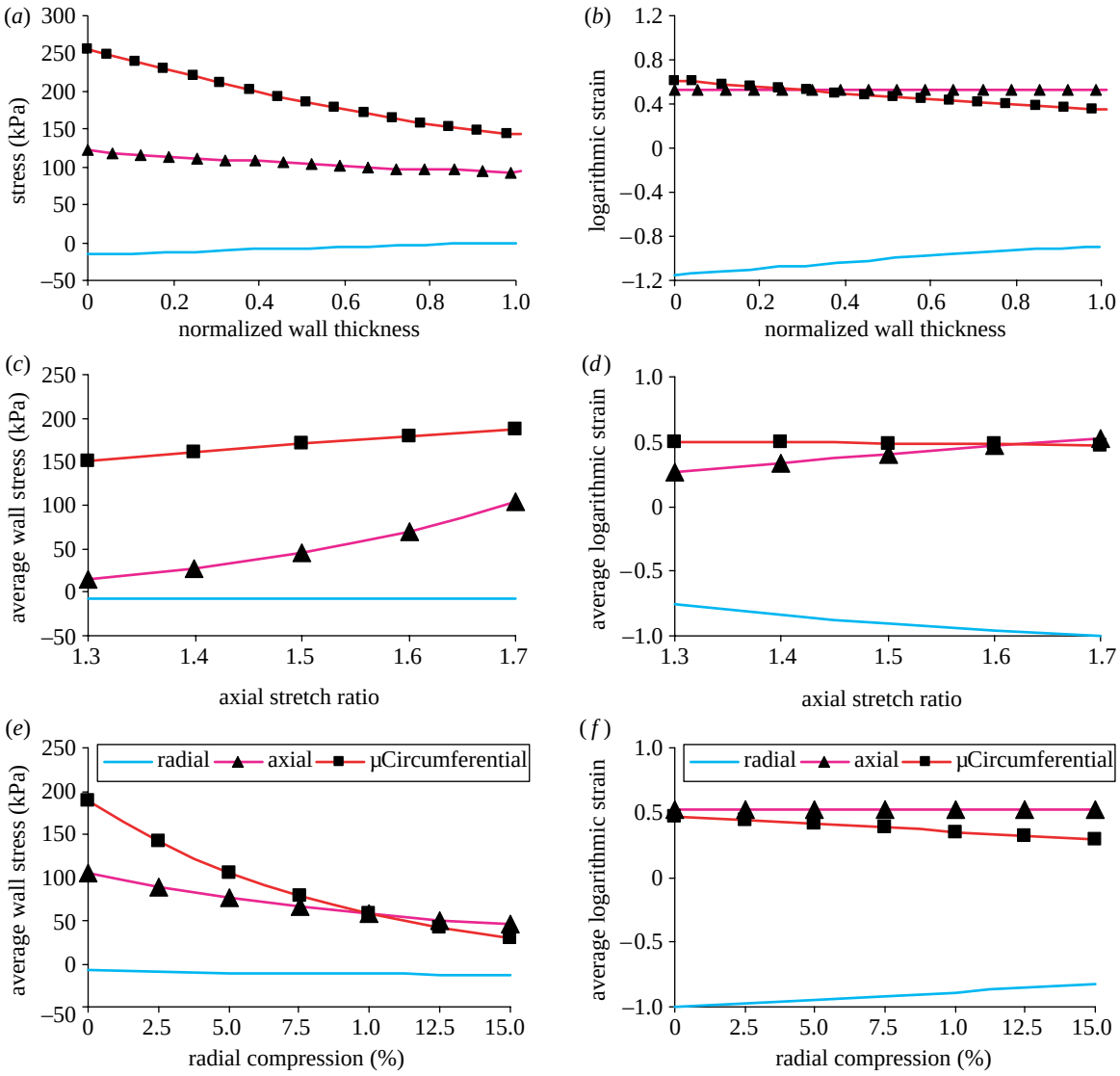

Figure 12. (*a*) Stress and (*b*) strain distributions in a rabbit thoracic aorta subjected to longitudinal stretch ratio of 1.7, pressure of 120 mmHg and effective opening angle of 71.4°. (*c*) Average stress and (*d*) average strain versus prescribed longitudinal stretch ratio at pressure of 120 mmHg. (*e*) Average stress and (*f*) average strain versus radial compression at internal pressure of 120 mmHg and longitudinal stretch ratio of 1.7. (Reproduced with permission from Zhang *et al.* (2005).)

intimately related. No analysis can be done without the constitutive equation. Conversely, the constitutive equation cannot be determined without the solution of a BVP. With the establishment of the Fung-type constitutive relation, we shall consider several BVPs.

5.1. Effect of zero-stress state

Prior to 1983, every study pointed to the existence of a stress concentration at the intima of the blood vessel and the subendocardium of ventricle, to the extent that the circumferential tension at the inner wall was much higher than that at the outer wall (Chuong & Fung 1983). The stress concentration implies high local energy consumption by the vessel or ventricle and consequently a high oxygen demand at the inner wall. The stress concentration at the inner wall was a direct consequence of the starting assumption that the unloaded (zero transmural pressure) blood vessel or ventricle is at the zero-stress state. The recognition of residual stress and strain reduced the stress concentration problem and simplified the stress–strain relation because it referred to a well defined state. Rachev & Greenwald provide a thorough review of the literature on residual strain of blood vessels (2003).

The implication of the circumferential residual strain was the 'uniform stress' hypothesis proposed by Fung (1983). The uniform stress hypothesis has been used by Takamizawa & Hayashi (1987, 1988) to predict the material constants of a strain energy density function and by others to understand arterial remodelling in response to changes in physical stress and strain (e.g. Rachev *et al.* 1996; Taber & Humphrey 2001). The three components of residual strains are shown in figure 11*a*. Figure 11*b* shows the distributions of circumferential stress in the vessel wall, with and without the circumferential residual strain. It is clearly seen that the residual strain greatly reduces the stress gradient. Although the residual stress at no-load state is relatively small in magnitude, it significantly contributes to the homogeneity of circumferential stress. The compressive and tensile circumferential

residual strains on the inner and outer sides of the vessel wall, respectively, compensate the tensile circumferential strain caused by the blood pressure. Hence, there is a significant reduction of stress gradient in the vessel wall (figure 11) due to the high nonlinearity of the stress–strain relation.

5.2. Effect of longitudinal pre-stretch

The existence of pre-stretch and longitudinal tethering was documented much earlier than circumferential residual strain (Fuchs 1900; Hesses 1926; Bergel 1961; Patel & Fry 1966; Patel & Vaishnav 1972; McDonald 1974). Numerous studies have quantified the degree of longitudinal shortening when a blood vessel is excised from the *in situ* condition as described earlier (see review in Guo & Kassab 2003). Although the effect of circumferential residual strain on the *in vivo* intramural stress distribution has been thoroughly investigated (see review in Rachev & Greenwald 2003), there are fewer studies on the effect of longitudinal pre-stretch (Gleason & Humphrey 2005*a*; Zhang *et al.* 2005).

Zhang *et al.* (2005) recently considered the effect of longitudinal pre-stretch on strain and stress distribution through a series of simulations with various longitudinal stretch ratios λ_z (the ratio of the longitudinal length of the vessel *in situ* to that *in vitro*) in the rabbit thoracic aorta (Chuong & Fung 1986). Figure 12*a*,*b* shows the principal Cauchy stress and logarithmic strain ($\log \lambda_c$, where λ_c is the circumferential stretch ratio) at $\lambda_z = 1.7$, respectively for the rabbit aorta. The transmural variations of stress and strain were averaged over the thickness of the wall and are shown in figure 12*c*,*d*, respectively, for various λ_z. The radial stress did not vary with the change in stretch ratio. It is seen that the circumferential and the longitudinal stresses both increase with an increase in stretch ratio (figure 12*c*). The increase in longitudinal stress, however, is much larger than the circumferential stress. As the λ_z increases, the longitudinal stress gradually reaches the magnitude of circumferential stress. Figure 12*d* reveals that the change of λ_z influences the radial and longitudinal strains significantly more than the circumferential strain. The radial strain, which is always compressive, becomes more compressive with an increase in λ_z. The longitudinal strain, which is completely prescribed by the longitudinal stretch ratio, is uniformly distributed in the vessel wall. The circumferential strain, which is dominated by the physiological pressure, appears to be almost independent of λ_z.

The longitudinal retraction or pre-stretch is small in the young and increases with postnatal growth and development as the vessels are stretched by body growth (Dobrin *et al.* 1975; Huang *et al.* 2006). Zhang *et al.* (2005) found that under the same physiological pressure, a more similar magnitude of circumferential and longitudinal stresses may be obtained by pre-stretching the vessel. Incidentally, the *in vivo* longitudinal stretch ratio of 1.7 yields similar circumferential and longitudinal strains, but not their stress counterparts (figure 12*c*,*d*) in the rabbit aorta.

The numerical results indicate that the increase of stretch ratio reduces the circumferential strain slightly, which makes the blood vessel 'stiffer'. The observation that longitudinal stretch increases the circumferential stiffness of a blood vessel has been previously confirmed experimentally by numerous studies (Cox 1975; Vaishnav & Vossoughi 1983; Weizsacker *et al.* 1983; Dobrin 1986; Humphrey *et al.* 1993; Pandit *et al.* 2005).

5.3. Effect of surrounding tissue

All blood vessels receive some perivascular support from the surrounding tissue. Some vessels such as pulmonary arteries receive little support while skeletal, myocardial or vertebral vessels are much more constrained (see review in Fung, 1983). To gain insight into the effect of radial constraint, Zhang *et al.* (2004, 2005) applied various displacement boundary conditions to constrain the outer surface to different extents, while keeping the internal pressure at 120 mmHg and the stretch ratio at 1.7. Figure 12*e*,*f* shows the intramural distribution of stress and strain, respectively, when the outer radius is compressed by various degrees. It is noted that the effect of radial constraint is to increase the radial stress but decrease the tensile longitudinal and circumferential stresses significantly. The simulation results indicate that the wall stress (especially the circumferential stress, see figure 12*e*) can be considerably reduced by an external constraint which effectively reduces the transmural pressure difference.

In the aorta, a 10% radial constraint results in similar values of circumferential and longitudinal stresses but not the strains (figure 12*e*,*f*). Hence, it appears that the aorta cannot have simultaneous uniformity between circumferential and longitudinal stresses and strains, which is in contrast to the coronary artery (Zhang *et al.* 2005). Since the geometry, residual strain and physiological loading are similar for the two vessel types, the difference lies in the material properties. We expect that the proximity of circumferential and longitudinal strain is more physiological since the thoracic aorta is not as radially compressed as the coronary artery (Hamza *et al.* 2003). Incidentally, Guo & Kassab (2003) have found the radial compression to be less than 5% for the mouse thoracic aorta which suggests a bi-axially similar strain (figure 12*f*).

6. STRUCTURE–FUNCTION RELATION

6.1. Mechanical homeostasis

Homeostasis is a very old axiom in physiology and medicine. In 1865, Claude Bernard stated that the 'constancy of the internal milieu was the essential condition to a free life' (Bernard 1957). In the past two decades, the existence of a homeostatic state of stress and strain in the CV system has received a great deal of attention. This surge of interest stems, in part, from the desire to understand growth and remodelling of blood vessels in response to changes in physical stress and strain. The 'uniform circumferential stress' hypothesis has emerged as one of the physical principle that

dictates the vascular response in hypertension. The increase in pressure leads to an increase in circumferential stress, which causes the vessel to chronically adapt with a proportional increase in thickness-to-radius ratio. Hence, the circumferential stress returns to the homeostatic state as per Laplace's equation (Wolinsky 1971, 1972; Vaishnav *et al.* 1990; Matsumoto & Hayashi 1994; Kassab *et al.* 2002). In addition to the uniform circumferential stress hypothesis, we have recently found that the circumferential strain (computed in reference to the zero-stress state) responds faster and recovers more quickly than the circumferential stress in the rat femoral artery (Lu *et al.* 2001) and pig common bile duct (CBD; Dang *et al.* 2004). Hence, the circumferential strain appears to be well regulated. The observed growth and remodelling processes that tend to restore the stresses and strains to some 'set values' support the hypothesis of a 'homeostatic' state of these parameters. We shall discuss these hypotheses in greater detail below.

6.1.1. Uniform shear hypothesis. The remodelling of blood vessels in response to flow-overload obeys the constant wall shear stress (WSS) hypothesis (Lu *et al.* 2001). This principle implies that the volumetric flow rate is proportional to the cube of the vessel radius assuming a laminar, incompressible, Newtonian flow through a rigid cylindrical vessel (Kassab & Fung 1995). Hence, in order to maintain a constant WSS, the cube of radius must increase in proportion to the increase in blood flow. Blood vessels can accommodate such a change in vessel radius at two levels: acutely through vasoactive mechanisms (flow-dependent constriction or dilation), and chronically by remodelling vascular caliber (Kamiya & Togawa 1980; Zarins *et al.* 1987).

Kamiya *et al.* (1984) have previously collected diameter and velocity data from the literature and estimated the WSS in the arterial system. They concluded that despite an approximately eight order of magnitude difference in flow rate in the arterial tree (aorta to pre-capillary arterioles), the WSS varies by about a factor of two (approx. 10–20 dyne cm^{-2}). Furthermore, the uniformity of WSS is restored even when blood flow is perturbed such as in flow-overload (Kamiya & Togawa 1980) or in flow-reduction (Langille & O'Donnell 1986). In summary, it has been observed that the vessel will remodel its lumen diameter so as to return the WSS to the homeostatic value (see review in Lu *et al.* 2001). The mechano-transduction responsible for this regulation has been the subject of great interest (see review in Davies 1995).

6.1.2. Uniform circumferential stress hypothesis. The blood pressure is primarily opposed by the forces of elastin, collagen and smooth muscle cells that are oriented to form well defined layers (see review in Rhodin 1979). Thick elastin bands form concentric lamellae while finer elastin fibres form networks between lamellae. The collagen fibres are distributed circumferentially in the interstices. In a comparative study of aorta from various species ranging from mouse to pig, Wolinsky & Glagov (1967) found that the total number of medial lamellar units is proportional to the aortic diameter. Hence, despite a large variation in aortic diameter, the average tension per lamellar unit of an aortic media is fairly constant.

The concept of average wall stress, tension divided by wall thickness, is theoretically more appropriate than tension for a thick walled vessel. Hence, the 'uniform tension' hypothesis was generalized into a uniform stress hypothesis as the principle that dictates the remodelling of arteries in hypertension (Wolinsky 1971, 1972; Vaishnav *et al.* 1990; Matsumoto & Hayashi 1994). It has been observed that the wall thickness-to-radius ratio increases in proportion to the increase in pressure such that the circumferential average wall stress is restored after some period of growth and remodelling. Hence, this hypothesis presupposes a homeostatic state of stress.

6.1.3. Uniform circumferential strain hypothesis. Our group has recently examined the uniform stress hypothesis in a flow-overload model of an arterial-venous fistula (Lu *et al.* 2001) and a pressure-overload model of CBD post obstruction (Duch *et al.* 2002; Dang *et al.* 2004). The time course of change of stress and strain was determined over a 12 weeks period in the a-v fistula and 32 days period in the obstructed CBD. Indeed, we found that the remodelling principle is consistent with normalization of average circumferential stress in the vessel wall. We found that strain, however, reached its peak sooner and normalized faster than stress. Hence, we conclude that the vessel appears more 'sensitive' to changes in strain. This implies the existence of a homeostatic state of strain.

6.1.4. Uniformity of strain throughout the CV system. Guo & Kassab (2004) recently determined the distribution of circumferential stress and strain along the porcine aorta and throughout the coronary arterial tree. They showed that the stretch ratio (circumference of the artery at physiological loading relative to the zero-stress state) and average wall stress varied from 1.2–1.6 to 10–150 kPa, respectively, along the aorta and the entire left anterior descending coronary arterial tree (more than three orders of magnitude difference in vessel diameters). The relative uniformity of circumferential stretch ratio from the proximal aorta to a 10 μm arteriole implies that the vascular system closely regulates the degree of deformation.

It should be noted, however, that the average circumferential wall stress reported does not correspond to the cell stress. In larger vessels where the average wall stress is higher (approx. 150 kPa), it is generally assumed that the cells are bearing a small fraction of the load because of the abundance of the load-bearing extracellular matrix (ECM). If we assume a constrained mixture model (Gleason & Humphrey 2005*b*) where the all components undergo the same strain but the stresses are additive, this implies that the cell stress is much less than the average wall stress. In smaller vessels where the average wall stress is significantly lower (approx. 10 kPa), the cell stress

would be closer to the average wall stress because there is much less ECM. Future studies are needed to compute the cellular stresses in small and large vessels to clarify cellular mechanics in mechanotransduction. The molecular mechanism responsible for the transduction of physical stimulus into a biochemical event remains as one of the most exciting areas of biomechanics research.

6.1.5. What is the stimulus for mechanotransduction? It has not been possible to establish whether blood vessels respond to stress or strain because it is difficult to experimentally separate the two mechanical stimuli. Stress and strain are intimately related through the material properties of the vessel wall (constitutive relation) and hence it is difficult to change one without affecting the other. We postulate that strain or possibly strain rate is the stimulus for mechano-transduction based on the premise that forces transmitted via individual proteins cause conformational changes that alter their binding affinity to other intracellular molecules. The force transmission may occur either at the site of cell adhesion or within the stress-bearing members of the cytoskeleton. The altered equilibrium state can subsequently initiate a biochemical signalling cascade or produce a local structural change. Since conformational change of a molecule or enzyme is inherently related to deformation, it is likely that chemical kinetics is affected by deformation. Stress, on the other hand, may be a driving force for transport processes.

There is significant data in the literature that supports the existence of stretch or deformation-activated ion channels in the vascular system (see review in Sachs 1988). Specifically, stretch-sensitive calcium ion channels have been identified and studied in endothelial cells (Naruse & Sokabe 1993; Hoyer *et al.* 1997; Naruse *et al.* 1998; Murase *et al.* 2001). Experiments that use micro-pipettes to stretch an endothelial cell membrane show the degree of stretch or deformation is related to the opening of transmembrane cation channels. The major effect of the activation of these mechano-sensitive ion channels is the influx of calcium and hence the depolarization of the cell. Moreover, there is a causal relation between mitogen activated protein kinase molecules of endothelial cells and both shear stress and cyclic strain (Tseng *et al.* 1995; Azuma *et al.* 2000).

6.1.6. Uniform transmural strain hypothesis. Fung & Liu (1992*a*,*b*) have previously shown that one of the implications of the existence of the residual strain is to make the transmural strain distribution more uniform. This was demonstrated in ileal, medial plantar and pulmonary arteries of the rat. We have tested this hypothesis along the entire length of the aorta (Guo *et al.* 2002). Our results show that the negative inner and positive outer residual strains lead to a uniform transmural strain distribution in the loaded state throughout the length of the aorta. This uniformity of transmural strain has important physiological implications (Fung & Liu 1992*a*,*b*).

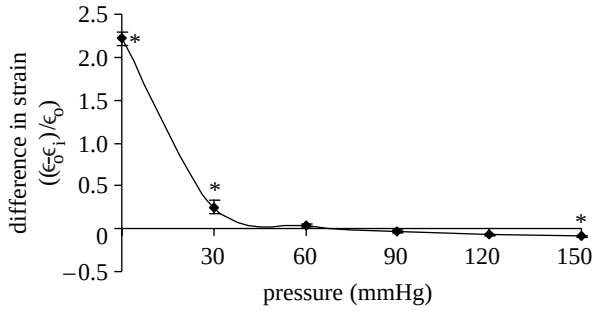

Figure 13. The variation of the difference in strain for the inner strain (ϵ_i) and outer strain (ϵ_o) with different pressures. The difference in strain was computed using the expression: $(\epsilon_o - \epsilon_i)/\epsilon_o$. *Denotes a value which is statistically different from zero. (Reproduced with permission from Guo & Kassab (2003).)

Guo & Kassab (2003) examined the effect of pressure on the uniformity of transmural strain. The difference between outer and inner strain is shown in figure 13. At zero-pressure, the values correspond to the residual strain. Outer residual strain is tensile while inner strain is compressive. Hence, the difference is fairly large as shown in figure 13. As the vessel is pressurized, the outer strain remains larger than the inner strain at a pressure of 30 mmHg. At 60 mmHg, the difference in transmural strains is not statistically significant. This remains to be the case until the pressure is increased to a value of 150 mmHg where the inner strain exceeds the outer strain. These results have important implications for hypertension where the increase in pressure may be well above 150 mmHg. The resulting gradient in transmural strain may be a stimulus for growth and remodelling (Kassab *et al.* 2002).

6.2. Vessel growth and remodelling

Stress and strain are intimately related to tissue function, growth and remodelling. Hence, a thorough understanding of the stress and strain state in the normal vessel wall can be used as a physiological reference state. The solution of BVPs reveals that distributions of stresses and strains become more uniform when the longitudinal pre-stretch is considered and the outer surface is restrained or compressed by the surrounding tissues. Hence, at the *in vivo* condition, residual strains in the circumferential, longitudinal and radial directions and surrounding tissue all help to maintain biaxial strain homogeneity or uniformity in the vessel wall. This may be the mechanical homeostasis of the vessel wall. Initiation of atherosclerosis or other vascular dysfunctions may be caused by perturbations of the mechanical homeostasis. Hence, the physical principle that dictates the growth and remodelling of the vessel wall is to restore the homeostatic mechanical state.

The ability of living tissues to adapt to altered mechanical loading conditions makes them very different from inanimate objects. It has been shown that stress and strain are the major stimuli for growth and remodelling (Kassab *et al.* 2002). For example, arteries change their structures, compositions, and

material properties when blood pressure increases (Fung 1993). The increase in residual strain in blood vessels in response to hypertension has been well documented (see review in Fung 1993). It is hypothesized that the increase in opening angle and accompanying residual strain serves to maintain a uniform stress and strain gradients despite the hypertension (Fung & Liu 1989). Theoretical models have also been developed to account for the stress-dependent adaptation of arteries (e.g. Rachev *et al.* 1996; Taber & Humphrey 2001). Several studies have examined the effects of longitudinal pre-stretch on cellular tissue growth and remodelling *in vivo* and *ex vivo* (Jackson *et al.* 2002; Clerin *et al.* 2003; Han *et al.* 2003). It was concluded that the growth restores the longitudinal strain while maintaining similar material properties. In a computational study, Gleason & Humphrey (2005*a*,*b*) used a mathematical growth and remodelling model to predict similar findings.

6.3. Postnatal development

Postnatal development involves tremendous growth and remodelling. At the time of birth, the major hemodynamic changes include an increase of CO and flow heterogeneity along the aorta, as well as an immediate increase in systemic blood pressure (Heymann *et al.* 1981). During early growth and development, the peripheral tissues continuously increase demand for blood flow as the blood pressure increases to accommodate those flows for several weeks (Langille 1993, 1995; Wiesmann *et al.* 2000).

The study of the changes of the geometry and mechanical properties during postnatal development is particularly important to understand the mechanisms of vascular adaptation in response to changes in physical stress. The pressure-induced circumferential wall tension and flow-induced WSS regulate the remodelling of the wall thickness and the diameter of the aorta, respectively (Langille 1995). Numerous studies have investigated the morphological, structural and biochemical changes of the aorta during development as well as the relation between these changes and the mechanics of the aorta (Berry *et al.* 1975; Langille 1993; Davis 1995; Saini *et al.* 1995; Wong & Langille 1996; Marchii & Becker 1997; Wells *et al.* 1998; Katsuda *et al.* 2002; Huang *et al.* 2006). These studies confirm that the aorta increases its lumen, wall thickness and mechanical stiffness during development.

6.3.1. Pressure and flow-induced remodelling. The first two weeks of the mouse life is characterized by simultaneous changes of blood pressure and CO. The mean arterial pressure increases from approximately 30 to 80 mmHg during postnatal development and reaches the adult value at two weeks of age in the C57BL/6 mice (Huang *et al.* 2006). The CO has been shown to increase linearly in the first four weeks of life of the same strain of mouse (Wiesmann *et al.* 2000). Hence in addition to the hormonal changes in the first two weeks of life, the mouse aorta experiences changes in both blood pressure and blood flow, with the changes of flow being significantly higher than those of pressure.

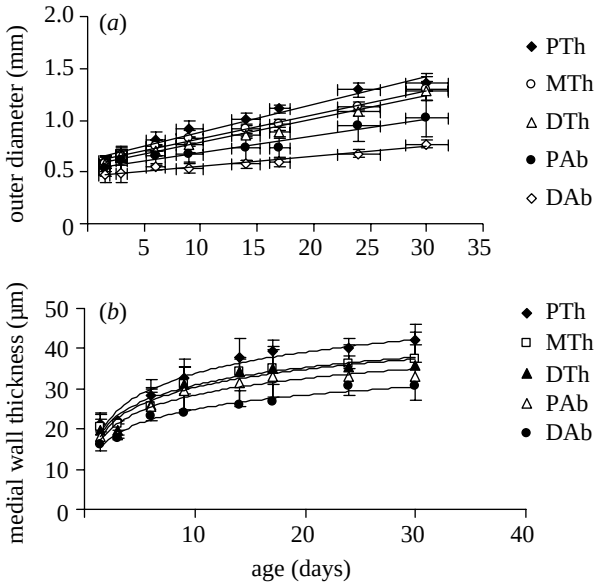

Figure 14. The variation of the (*a*) outer diameter and the (*b*) medial wall thickness along the longitudinal location of the aorta with age. PTh, MTh, DTh, PAb and DAb represent proximal thoracic, middle thoracic, distal thoracic, proximal abdominal and distal abdominal aorta, respectively. (Reproduced with permission from Huang *et al.* (2006).)

Numerous studies have demonstrated that changes in blood pressure are associated with changes in wall thickness. Aortic wall thickening was observed during development (Davis 1995; Olivetti *et al.* 1980; Marchii & Becker 1997) and it was attributed to the medial tissue accumulation of elastin, collagen and smooth muscle cells. The wall thickness increases rapidly during the first two weeks of the mouse life (Huang *et al.* 2006). Huang *et al.* (2006) found that the growth of the wall thickness is not uniform along the aorta during development. The thoracic aorta grows faster than the abdominal, where the proximal aorta grows the fastest and the distal aorta grows the slowest.

The major blood flow changes at the time of birth include a dramatic increase in pulmonary flow because of the postnatal loss of the placental circulation. Furthermore, there is a dramatic decline in blood flow in the abdominal aorta due to the closure of the umbilical arteries at birth (Heymann *et al.* 1981). Langille *et al.* (1990) found the abdominal aortic external diameter in the period between 4 and 14 days postpartum was reduced significantly as compared with *in utero* values. Huang *et al.* (2006) showed a linear relationship in the outer (figure 14*a*) and inner diameter (data not shown) of the aorta with age. The growth rate of both the outer and the inner diameters of thoracic and abdominal aorta are different during the first two weeks of life (Huang *et al.* 2006).

6.3.2. Flow-induced remodelling. Although the blood pressure plateaus at two weeks of age, the CO continues to increase linearly between weeks three and four of age (Wiesmann *et al.* 2000). Interestingly, the growth of the wall thickness of the aorta appears to level off when the

mouse reaches two weeks of age (figure 14*b*). This observation is consistent with hypertension-induced wall hypertrophy verified by previous studies (Matsumoto & Hayashi 1994; Laurent 1995). It has been previously demonstrated that the growth rate of the medial CSA between the thoracic and the abdominal aorta were different (Langille *et al.* 1990). This suggests that the aorta radially transforms from a relatively thin cylindrical tube to a thicker structure where the thickness tapers along the length of the aorta during postnatal growth (Huang *et al.* 2006).

Figure 14*a* shows that the outer diameter of the aorta increases linearly with age within the first four weeks of life, with the proximal thoracic aorta growing the fastest, and the distal abdominal aorta growing the slowest (Huang *et al.* 2006). This implies that the blood flow increases the most at the proximal aorta. This difference in flow circumferentially transforms the aorta from a relatively cylindrical tube to a tapering structure after birth.

6.3.3. Longitudinal growth and remodelling. During development, the body length grows faster than the aorta as shown in figure 15*a*. The body length grows the fastest while the aorta grows the slowest. This implies that the aorta is subjected to a distending longitudinal force during growth, which becomes significant after three weeks of age (Huang *et al.* 2006). The rate of growth of aorta is 0.72 mm d^{-1} or 4% of total length per day. In an *ex vivo* system, Clerin *et al.* (2003) axially stretched porcine carotid arteries in organ culture for several weeks. They found a limit (approx. 8% per day) to the degree of longitudinal stretch that could be imposed while maintaining normal structure and function. Hence, the physiological stretch of aorta during normal development is well below the tolerance of the porcine carotid arteries.

6.3.4. Changes in opening angle during postnatal development. Fung (1990) has previously proposed that the remodelling of the zero-stress state is an index of the non-uniformity of growth and remodelling. Fung & Liu showed that hypertension induces growth of intima that exceeds that of the adventitia (Fung & Liu 1989, 1992*a*,*b*; Liu & Fung 1989). Consequently, the vessel sector, in the zero-stress state, shows an outward bend and hence an increase in the opening angle. Conversely, Lu *et al.* (2001) showed that flow-overload induces growth of adventitia that exceeds that of intima. Hence, the vessel sector bends inward and decreases the opening angle. In summary, hypertension and flow-overload have opposing effects on the opening angle. In models of simultaneous hypertension and flow-overload, the effects of opening angle are nearly conciliatory (Kassab *et al.* 2002).

Huang *et al.* (2006) results are consistent with the previous findings if we consider the changes in pressure and flow. In the thoracic aorta, the change in flow dominates the change in pressure and hence the opening angle decreases during development. In the abdominal aorta, however, the changes in pressure and flow are fairly similar and hence the effect is conciliatory. In future studies, it will be interesting to consider the effect of change in zero-stress state on the transmural distribution of intramural stress and strain.

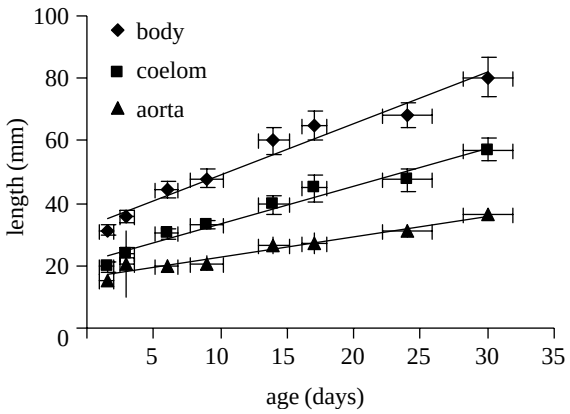

Figure 15. The variation of the length of the (*a*) body, coelom and aorta and (*b*) global axial stretch ratio with age. '*' denotes $p<0.05$ when compared with other groups. (Reproduced with permission from Huang *et al.* (2006).)

6.3.5. Changes in mechanical properties during postnatal development. The elastin and collagen are thought to contribute to the elastic properties at low and moderate blood pressures, and high pressures, respectively (Berry *et al.* 1975; Silver *et al.* 1989). During development, there is an uneven growth of each of micro-structural components, with increases in collagen > elastic laminae > muscle cells (Olivetti *et al.* 1980). The collagen content is lower and the elastic fibre content is higher in the thoracic as compared with the abdominal aorta which implies the thoracic aorta is more compliant than the abdominal aorta (Fischer & Llaurado 1966).

At birth when the pressure is low, the elastic modulus (figure 16*a*) and the compliance (figures 16*b* and 17*a*,*b*) are small and fairly uniform along the entire length of the aorta. As the pressure increases, the aorta becomes more elastic. Furthermore, the aorta becomes mechanically heterogeneous with the proximal region near the heart being the most compliant and the distal region least compliant. This is a functional adaptation of the aorta to serve as a windkessel.

Similarly, the data on circumferential Cauchy stress shows uniformity along the aorta during the first post-partum period (Langille *et al.* 1990; Huang *et al.* 2006). Thereafter, the stress imposed on the proximal aorta is higher than the distal abdominal aorta (figure 18*a*). Hence, the Cauchy stress becomes heterogeneous along the length of the aorta during postnatal growth and development.

6.3.6. Tendency for strain homeostasis. The issue of mechanical homeostasis can be explored from the data by Huang *et al.* (2006) in conjunction with a previous study by Guo & Kassab (2003) on mice of age 10 weeks. Huang *et al.* (2006) found a rapid (3–4 folds) increase of the circumferential Cauchy stress in the first 30 days of age (figure 18*a*). The change in stress at 10 weeks in comparison to 30 days is significant. Hence, the

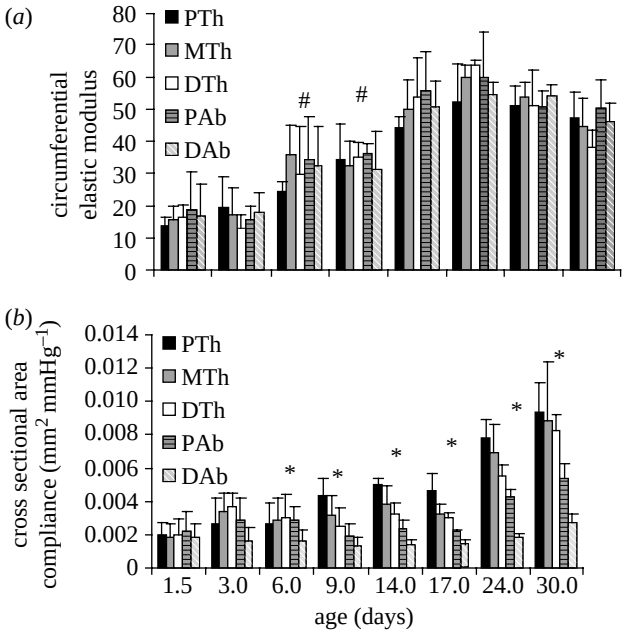

Figure 16. (*a*) The circumferential elastic modulus and (*b*) the static cross-sectional area compliance ($\Delta CSA/\Delta P$) for different segments of aorta. '#' denotes significant difference when comparing with other age group. PTh, MTh, DTh, PAb and DAb denote proximal thoracic, middle thoracic, proximal thoracic, proximal abdominal and distal abdominal aorta, respectively. '*' denotes significant differences when comparing different segments along the aorta. (Reproduced with permission from Huang *et al.* (2006).)

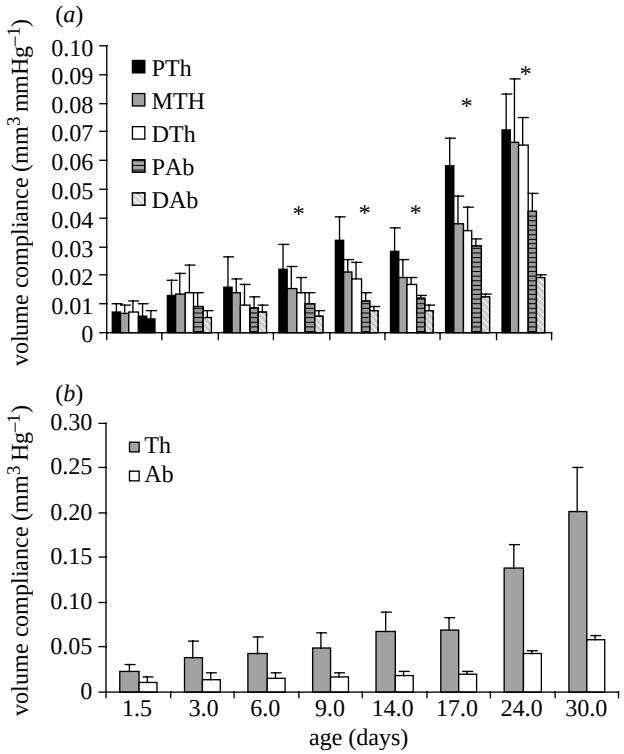

Figure 17. The volume compliance for different segments of the (*a*) aorta and the (*b*) thoracic and abdominal aorta. PTh, MTh, DTh, PAb and DAb denote proximal thoracic, middle thoracic, proximal thoracic, proximal abdominal and distal abdominal aorta, respectively. '*' denotes significant difference when compared with different segments along the aorta. (Reproduceed with permission from Huang *et al.* (2006).)

circumferential stress continues to increase. The circumferential elastic modulus of the mouse aorta increases gradually from the time of birth and reaches a relatively constant value after two weeks of age (figure 16*a*). These results suggest that the aorta becomes stiffer with development, with stiffness of abdominal > thoracic aorta. This is consistent with the micro-structural remodelling described earlier. The modulus also continues to increase from 30 days to 10 weeks, although the change is not statistically significant (figure 18*b*). The strain, however, is unchanged at 10 weeks relative to 30 days (figure 18*b*). Indeed, the circumferential Green strain of the mouse aorta reached the adult value at the age of two weeks as shown in figure 18*b*. The time scale to reach a uniform strain is relatively short.

At birth, the WSS is significantly higher than physiological values and decreases linearly during development (Huang *et al.* 2006). This is certainly a strong stimulus for the remodelling of the lumen of the aorta. Interestingly, the WSS is essentially normalized at 30 days. In conclusion, it appears that the circumferential strain and WSS normalize faster than the circumferential stress (Huang *et al.* 2006). Hence, the WSS and strain appear to attain their homeostatic values early in life.

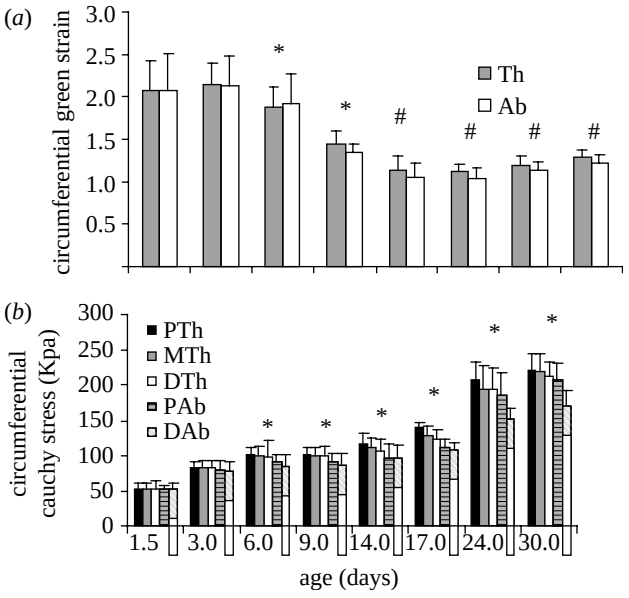

Figure 18. The variation of the (*a*) circumferential Green strain and the (*b*) Cauchy stress with age. Th and Ab represent thoracic and abdominal aorta, respectively. '*' denotes significant difference when comparing different segments along the aorta. '#' denotes significant difference when comparing thoracic and abdominal aorta. (Reproduced with permission from Huang *et al.* (2006).)

7. FUTURE DIRECTIONS

Biological tissues have unique features that include the ability to grow, change and reproduce; the process of aging and dying, and the existence of an intricate

system of feedback and control. The mathematical description of growth and resorption of tissues as functions of stress and strain is an extremely important area of research and may serve as a foundation for tissue engineering. Another important direction of research is to study the ultra-structure of the tissues in order to formulate a theory of the mechanical properties on the basis of micro-structure. The coupling of imaging methods such as MPM that enables the identification of elastin and collagen fibres of the vessel wall under mechanical loading with numerical methods that take advantage of modern computational capability to deal with the complex micro-structural geometry and boundary conditions should advance this important area of research. Finally, the need for a constitutive equation for the vascular smooth muscle is critical. Without it, we cannot develop a mathematical theory of circulatory regulation and control. This area of CV biomechanics research should be a high priority.

The author acknowledges the fruitful collaborations with Drs Xiaomei Guo, Yi Huang, Xiao Lu, Wei Zhang, Katerina Zoumi, Bruce Tromberg, Robert Mattrey and Satya Atluri in these studies. This research was supported in part by the National Institute of Health-National Heart, Lung and Blood Institute grant 5 R29 HL55554, by the National Science Foundation grant no. 9978199 and by the American Heart Association 0140036N.

REFERENCES

Abe, H., Hayashi, K. & Sato, M. (eds) 1996 *Data book on mechanical properties of living cells, tissues and organs*. Tokyo, Japan: Springer.

Airaksinen, K. E. J., Salmela, P. I., Linnaluoto, M. K., Iläheimo, M. J., Ahola, K. & Ryhänen, L. J. 1993 Diminished arterial elasticity in diabetes: association with fluorescent advanced glycosylation end products in collagen. *Cardiovasc. Res.* **27**, 942–945.

Alavi, A., Gupta, N., Alberini, J. L., Hickeson, M., Adam, L. E., Bhargava, P. & Zhuang, H. 2002 Positron emission tomography imaging in nonmalignant thoracic disorders. *Semin. Nucl. Med.* **32**, 293–321. (doi:10.1053/snuc.2002.127291)

Arnett, D. K., Evans, G. W. & Riley, W. A. 1991 Artery stiffness: a new CV risk factor? *Am. J. Epidemiol.* **140**, 669–682.

Arruda, E. M. & Boyce, M. C. 2004 A three-dimensional constitutive model for the large stretch behavior of rubber elastic materials. *J. Mech. Phys. Solids* **41**, 398–412.

Atluri, S. N. 1984 Alternate stress and conjugate strain measures, and mixed variational formulations involving rigid rotations, for computational analyses of finitely deformed plates and shells. Part I: theory. *Comput. Struct.* **18**, 93–116. (doi:10.1016/0045-7949(84)90085-3)

Avolio, A. P., Chen, S., Wang, R., Zhang, C. L., Li, M. F. & O'Rourke, M. F. 1983 Effects of aging on changing arterial compliance and left ventricular load in a northern chinese urban community. *Circulation* **68**, 50–58.

Azuma, T. & Hasagawa, M. 1971 A rheological approach to the architecture of arterial walls. *Jpn. J. Physiol.* **21**, 37–47.

Azuma, T. & Oka, S. 1971 Mechanical equilibrium of blood vessel walls. *Am. J. Physiol.* **221**, 1310.

Azuma, N., Duzgun, S. A., Ikeda, M., Kito, H., Akasaka, N., Sasajima, T. & Sumpio, B. E. 2000 Endothelial cell response to different mechanical forces. *J. Vasc. Surg.* **32**, 789–794. (doi:10.1067/mva.2000.107989)

Barbee, R. W., Perry, B. D., Re, R. N. & Murgo, J. P. 1992 Microsphere and dilution techniques for the determination of blood flows and volumes in conscious mice. *Am. J. Physiol. Regul. Integr. Comp. Physiol.* **263**, R728–R733.

Belz, G. G. 1995 Elastic properties and Windkessel function of the human aorta. *Cardiovasc. Drugs Ther.* **9**, 73–83. (doi:10.1007/BF00877747)

Bergel, D. H. 1961 The static elastic properties of the arterial wall. *J. Physiol.* **156**, 445–457.

Bernard, C. 1957 *An introduction to the study of experimental medicine*. New York, NY: Dover Publications, Inc.

Berry, C. L., Greenwald, S. E. & Rivett, J. F. 1975 Static mechanical properties of the developing and mature rat aorta. *Cardiovasc. Res.* **9**, 669–678.

Bischoff, J. E., Arruda, E. M. & Grosh, K. 2002 A microstructural based orthotropic hyperelastic constructive law. *ASME J. Appl. Mech.* **69**, 570–579.

Boutouyrie, P., Tropeano, AI, Asmar, R., Gautier, I., Benetos, A., Lacolley, P. & Laurent, S. 2002 Aortic stiffness is an independent predictor of primary coronary events in hypertensive patients: a longitudinal study. *Hypertension* **39**, 10–15. (doi:10.1161/hy0102.099031)

Burkitt, G. H., Young, B. & Health, J. W. 1993 *Wheater's functional histology: a text and colour atlas*. New York, NY: Churchill Livingstone.

Chien, S. 1978 Transport across arterial endothelium. *Prog. Hemost. Thromb.* **4**, 1–36.

Chuong, C. J. & Fung, Y. C. 1983 Three-dimensional stress distribution in arteries. *J. Biomech. Eng.* **105**, 268–274.

Chuong, C. J. & Fung, Y. C. 1986 On residual stresses in arteries. *J. Biomech. Eng.* **108**, 189–192.

Clerin, V., Nichol, J. W., Petko, M., Myung, R. J., Gaynor, J. W. & Gooch, K. J. 2003 Tissue engineering of arteries by directed remodeling of intact arterial segments. *Tissue Eng.* **9**, 461–472. (doi:10.1089/107632703322066642)

Coley, D. A. 1999 *An introduction to genetic algorithms for scientists and engineers*. Hackensack, NJ: World Scientific Publishing Company.

Cox, R. H. 1975 Anisotropic properties of the canine carotid-artery *in vitro*. *J. Biomech.* **8**, 293–300. (doi:10.1016/0021-9290(75)90081-0)

Dang, Q., Duch, B., Gregersen, H. & Kassab, G. S. 2004 Indicial response of growth and remodeling of common bile duct post obstruction. *Am. J. Physiol. Gastrointest. Liver Physiol.* **286**, G420–G427. (doi:10.1152/ajpgi.00306.2003)

Dart, A. M., Lacombe, F., Yeoh, J. K., Cameron, J. D., Jenning, G. L., Laufer, E. & Esmore, D. S. 1991 Aortic distensibility in patients with isolated hypercholesterinemia, coronary artery disease or cardiac transplant. *Lancet* **338**, 270–277. (doi:10.1016/0140-6736(91)90415-L)

Davies, P. F. 1995 Flow-mediated endothelial mechanotransduction. *Physiol. Rev.* **75**, 519–560.

Davis, E. C. 1995 Elastic lamina growth in the developing mouse aorta. *J. Histochem. Cytochem.* **43**, 1115–1123.

DeBakey, M. E., Lawrie, G. M. & Glaeser, D. H. 1985 Patterns of atherosclerosis and their surgical significance. *Ann. Surg.* **201**, 115–131.

Decraemer, W. F., Maes, M. A. & Vanhuyse, V. J. 1980 An elastic stress–strain relation for soft biological tissues based on a structure model. *J. Biomech.* **13**, 463–468. (doi:10.1016/0021-9290(80)90338-3)

DiDonna, B. A. & Lubensky, T. C. 2005 Nonaffine correlations in random elastic media. *Condens. Mater.* **2**, 1–23.

Dobrin, P. B. 1986 Biaxial anisotropy of dog carotid-artery: estimation of circumferential elastic modulus. *J. Biomech.* **19**, 351–358. (doi:10.1016/0021-9290(86)90011-4)

Dobrin, P. B. & Doyle, J. M. 1970 Vascular smooth muscle and anisotropy of dog carotid artery. *Circ. Res.* **27**, 105–119.

Dobrin, P., Canfield, T. & Sinha, S. 1975 Development of longitudinal retraction of carotid arteries in neonatal dogs. *Experientia* **31**, 1295–1296. (doi:10.1007/BF01945788)

Duch, B. U., Andersen, H. L., Smith, J., Kassab, G. S. & Gregersen, H. 2002 Structural and mechanical remodeling of the common bile duct during experimental obstruction. *Neurogastroenterol. Mot.* **14**, 111–122. (doi:10.1046/j.1365-2982.2002.00310.x)

Dunn, T. 1965 Spontaneous lesions of mice. In *The laboratory animals* (ed. W. E. Rilein & J. R. McCoy), pp. 303–329. Springfiled, IL: Charles C Thomas.

Dzau, V. J. & Safar, M. E. 1988 Large conduit arteries in hypertension: role of the vascular enin-angiotensin system. *Circulation* **77**, 947–954.

Faraci, F. M. & Sigmund, C. D. 1999 Vascular biology in genetically altered mice: smaller vessels, bigger insight. *Circ. Res.* **85**, 1214–1225.

Festing, M. F. W. & Blackmore, D. K. 1971 Lifespan of specified-pathogen-free (MRC category 4) mice and rats. *Lab. Anim.* **5**, 179–192.

Fischer, G. M. & Llaurado, J. G. 1966 Collagen and elastin content in canine arteries selected from functionally different vascular beds. *Circ. Res.* **19**, 394–399.

Fuchs, R. F. 1900 Zur Physiologie und Wachstummsmechanik des blutgefassystems. *Arch. Ges. Physiol.* **28**, 7.

Fung, Y. C. 1983 What principle governs the stress distribution in living organisms? In *Biomechanics in China, Japan, and USA* (ed. Y. C. Fung, E. Fukada & J. J. Wang), pp. 1–13. Beijing, China: Science Press.

Fung, Y. C. 1984 *Biodynamics: circulation*. New York, NY: Springer.

Fung, Y. C. 1990 *Biomechanics: motion, flow, stress and growth*. New York, NY: Springer.

Fung, Y. C. 1993 *Biomechanics: mechanical properties of living tissues*, 2nd edn. New York, NY: Springer.

Fung, Y. C. 1996 New trends in biomechanics. Keynote Lecture. In *Proc. 11th Conf. on Engineering Mechanics* (eds Lin, Y. K. & Su, T. C.), pp. 1–15. Washington, DC: American Society of Civil Engineers.

Fung, Y. C. & Liu, S. Q. 1989 Change of residual strains in arteries due to hypertrophy caused by aortic constriction. *Circ. Res.* **65**, 1340–1349.

Fung, Y. C. & Liu, S. Q. 1992*a* Strain distribution in small blood vessels with zero-stress state taken into consideration. *Am. J. Physiol. Heart Circ. Physiol.* **262**, H544–H552.

Fung, Y. C. & Liu, S. Q. 1992*b* Change of zero-stress state of rat pulmonary arteries in hypoxic hypertension. *J. Appl. Physiol.* **262**, 2455–2470.

Fung, Y. C., Fronek, K. & Patitucci, P. 1979 Pseudoelasticity of arteries and the choice of its mathematical expression. *Am. J. Physiol.* **237**, H620–H631.

Fyfe, A. I., Qiao, J.-H. & Lusis, A. J. 1994 Immune-deficit mice develop typical atherosclerotic fatty streaks when fed an atherogenic diet. *J. Clin. Invest.* **94**, 2516.

Gillensen, T., Gillensen, F., Sieberth, H., Hanrath, P. & Heintz, B. 1995 Age-related changes in the elastic properties of the aortic tree in normotensive patients: investigation by intravascular ultrasound. *Eur. J. Med. Res.* **1**, 144–148.

Gleason, R. L. & Humphrey, J. D. 2005*a* Effects of a sustained extension on arterial growth and remodeling: a theoretical study. *J. Biomech.* **38**, 1255–1261. (doi:10.1016/j.jbiomech.2004.06.017)

Gleason, R. L. & Humphrey, J. D. 2005*b* A 2D constrained mixture model for arterial adaptations to large changes in flow, pressure and axial stretch. *Math. Med. Biol.* **22**, 347–369. (doi:10.1093/imammb/dqi014)

Goldberg, D. E. 1989 *Genetic algorithms in search, optimization and machine learning*. Reading, MA: Addison Wesley Publishing Company.

Grahn, D. 1972 Data collection and genetic analysis in the selection and study of rodent model systems in aging. In *Development of the rodent as a model system of aging* (ed. D. Gibson), pp. 55–65. Bethesda, MD: DHEW, Pub No (NIH) 72–121.

Green, A. E. & Adkins, J. E. 1960 *Large deformations and nonlinear continuum mechanics*. Oxford, UK: Oxford University Press.

Guo, X. & Kassab, G. S. 2003 Variation of mechanical properties along the length of the aorta inC57bl/6 mice. *Am. J. physiol. Heart Circ. Physiol.* **285**, H2614–H2622.

Guo, X. & Kassab, G. S. 2004 Distribution of stress and strain along the porcine aorta and coronary arterial tree. *Am. J. Physiol. Heart Circ. Physiol.* **286**, H2361–2368. (doi:10.1152/ajpheart.01079.2003)

Guo, X., Kono, Y., Mattrey, R. & Kassab, G. S. 2002 Morphometry and strain distribution of the C57BL/6J mouse aorta. *Am. J. Physiol. Heart Circ. Physiol.* **283**, H1829–H1837.

Guo, X., Lu, X. & Kassab, G. S. 2005 Transmural strain distribution in the blood vessel wall. *Am. J. Physiol. Heart Circ. Physiol.* **288**, H881–H86. (doi:10.1152/ajpheart.00607.2004)

Hales, S. 1733 *Statistical essays: containing Haemastaticks*. New York, NY: Hafner Publishing. Reprinted 1964

Hamza, L. H., Dang, Q., Lu, X., Mian, A., Molloi, S. & Kassab, G. S. 2003 Effect of passive myocardium on the compliance of porcine coronary arteries. *Am. J. Physiol. Heart Circ. Physiol.* **285**, H653–H660.

Han, H. C. & Fung, Y. C. 1991 Species dependence of the zero-stress state of aorta: pig versus rat. *J. Biomech. Eng.* **113**, 446–451.

Han, H. C. & Fung, Y. C. 1995 Longitudinal strain of canine and porcine aortas. *J. Biomech. Eng.* **28**, 637–641. (doi:10.1016/0021-9290(94)00091-H)

Han, H. C., Ku, D. N. & Vito, R. P. 2003 Arterial wall adaptation under elevated longitudinal stretch in organ culture. *Ann. Biomed. Eng.* **31**, 403–411. (doi:10.1114/1.1561291)

Hanahan, D. 1990 Transgenic mice as probes into complex systems. *Science* **246**, 1265–1275.

Hayashi, K. 1993 Experimental approaches on measuring the mechanical properties and constitutive laws of arterial walls. *J. Biomech. Eng.* **115**, 481–488.

Heints, B., Gillessen, T., Walkenhorst, F., vom Dahl, J., Dorr, R., Krebs, W., Hanrath, P. & Sieberth, H. G. 1993 Evaluation of segmental elastic properties of the aorta in normotensive and medically treated hypertensive patients by intravascular ultrasound. *J. Hypertens.* **11**, 1253–1258.

Hesses, M. 1926 Uber die pathologischen Veranderungen der Arterien der oberen extremitat. *Virchows Arch. Path. Anat. Physiol.* **261**, 225–252. (doi:10.1007/BF01891877)

Heymann, M. A., Iwamoto, H. S. & Rudolph, A. M. 1981 Factors affecting changes in the neonatal systemic circulation. *Annu. Rev. Physiol.* **43**, 371–383. (doi:10.1146/annurev.ph.43.030181.002103)

Hodes, R. J., Lakatta, E. G. & Mcneil, C. T. 1995 Another modifiable risk factor for CV disease? Some evidence points to arterial stiffness. *J. Am. Geriatr. Soc.* **43**, 581–582.

Holzapfel, G. A. & Gasser, T. C. 2000 A new constitutive framework for arterial wall mechanics and a comparative study of material models. *J. Elasticity* **61**, 1–48. (doi:10.1023/A:1010835316564)

Holzapfel, G. A. & Weizsacker, H. W. 1998 Biomechanical behavior of the arterial wall and its numerical characterization. *Comput. Biol. Med.* **28**, 377–392. (doi:10.1016/S0010-4825(98)00022-5)

Hoyer, J., Kohler, R. & Distler, A. 1997 Mechanosensitive cation channels in aortic endothelium of normotensive and hypertensive rats. *Hypertension* **30**(1 Pt 1), 112–19.

Huang, Y., Guo, X. & Kassab, G. S. 2006 Axial nonuniformity of geometric and mechanical properties of mouse aorta increase during postnatal growth. *Am. J. Physiol.* **290**, H657–H664. (doi:10.1152/ajpcell.00226.2005)

Hughes, H. C. 1986 Swine in cardiovascular research. *Lab. Anim. Sci.* **36**, 348–350.

Hughes, G. C., Post, M. J., Simons, M. & Annex, B. H. 2003 Translational physiology: porcine models of human coronary artery disease: implications for preclinical trials of therapeutic angiogenesis. *J. Appl. Physiol.* **94**, 1689–1701.

Humphrey, J. D. 1995 Mechanics of the arterial wall: review and directions. *Crit. Rev. Biomed. Eng.* **23**, 1–162.

Humphrey, J. D., Kang, T., Sakarda, P. & Anjanappa, M. 1993 Computer-aided vascular experimentation: a new electromechanical test system. *Ann. Biomed. Eng.* **21**, 33–43. (doi:10.1007/BF02368162)

Idiris, A., Alam, M. T. & Ikai, A. 2000 Speing mechanics of α-helical polypeptide. *Protein Eng.* **13**, 763–770. (doi:10.1093/protein/13.11.763)

Ito, H., Yamakoshi, K., Shimazu, H. & Togawa, T. 1977 Measurement of aortic compliance from the transthoracic admittance plethysmogram in the living dog. *Med. Biol. Eng. Comput.* **15**, 618–26.

Jackson, Z. S., Gotlieb, A. I. & Langille, B. L. 2002 Wall tissue remodeling regulates longitudinal tension in arteries. *Circ. Res.* **90**, 918–925. (doi:10.1161/01.RES.0000016481.87703.CC)

Kamiya, A. & Togawa, T. 1980 Adaptive regulation of wall shear stress to flow change in the canine carotid artery. *Am. J. Physiol.* **239**, H14–H21.

Kamiya, A., Bukhari, R. & Togawa, T. 1984 Adaptive regulation of wall shear stress optimizing vascular tree function. *Bull. Math. Biol.* **46**, 127–137. (doi:10.1016/S0092-8240(84)80038-5)

Kang, P. S. & Spain, J. W. 2005 Multidetector CT angiography of the abdomen. *Radiol. Clin. North Am.* **43**, 963–76.

Karr, C. L., Yakushin, I. & Nicolosi, K. 2000 Solving inverse initial-value boundary value problems via genetic algorithm. *Eng. Appl. Artif. Intell.* **13**, 625–633. (doi:10.1016/S0952-1976(00)00025-7)

Kassab, G. S. 2001 Analysis of coronary circulation: a bioengineering approach. In *Introduction to bioengineering* (ed. Y. C. Fung), pp. 93–105. Singapore, Singapore: World Scientific.

Kassab, G. S. & Fung, Y. C. 1995 The pattern of coronary arteriolar bifurcations and the uniform shear hypothesis. *Ann. Biomed. Eng.* **23**, 13–20. (doi:10.1007/BF02368296)

Kassab, G. S., Gregersen, H., Nielsen, S. L., Lu, X., Tanko, L. B. & Falk, E. 2002 Remodeling of the left anterior descending artery in a porcine model of supravalvular aortic stenosis. *J. Hypertens.* **20**, 2429–2437. (doi:10.1097/00004872-200212000-00023)

Katsuda, S., Waki, H., Yamasaki, M., Nagayama, T., O-Ishi, H., Katahira, K., Machida, N., Hasegawa, M. & Shimizu, T. 2002 Postnatal changes in the rheological properties of the aorta in Sprague-Dawley rats. *Exp. Anim.* **51**, 83–93. (doi:10.1538/expanim.51.83)

Khan, Z., Millard, R. W., Gabel, M., Walsh, R. A. & Hoit, B. D. 1999 Effect of congestive heart failure on *in vivo* canine aortic elastic properties. *J. Am. Coll. Cardiol.* **33**, 267–272. (doi:10.1016/S0735-1097(98)00530-0)

Langille, B. L. 1993 Remodeling of developing and mature arteries: endothelium, smooth muscle and matrix. *J Cardiovasc. Pharmacol.* **21**, S11–S17.

Langille, B. L. 1995 Blood flow-induced remodeling of the artery wall. In *Flow-dependent regulation of vascular function* (ed. J. A. Bevan, G. Kaley & G. Rubanyi), pp. 277–299. New York, NY: Oxford University Press.

Langille, B. L. & O'Donnell, F. 1986 Reductions in arterial diameter produced by chronic decreases in blood flow are endothelium-dependent. *Science* **231**, 405–47.

Langille, B. L., Brownlee, R. D. & Adamson, S. L. 1990 Perinatal aortic growth in lambs-relation to blood-flow change at birth. *Am. J. Physiol. Heart Circ. Physiol.* **259**, H1247–H1253.

Lanir, Y. 1983 Non-linear constitutive model for plain-weave composites,. *J. Biomech.* **16**, 1–12. (doi:10.1016/0021-9290(83)90041-6)

Laurent, S. 1995 Arterial wall hypertrophy and stiffness in essential hypertensive patients. *Hypertension* **26**, 355–362.

Laurent, S., Katsahian, S., Tropeano, A.-I., Gautier, I., Laloux, B. & Boutouyrie, P. 2003 Aortic stiffness is an independent predictor of fatal stroke in essential hypertension. *Stroke* **34**, 1203–1206. (doi:10.1161/01.STR.0000065428.03209.64)

Lehmann, E. D., Watts, G. F. & Gosling, R. G. 1992 Aortic distensibility and hypercholesterolaemia. *Lancet* **340**, 1171–1172. (doi:10.1016/0140-6736(92)93210-E)

Levy, B. I., Benessiano, J., Poitevin, P., Lukin, L. & Safar, M. E. 1985 Systemic arterial compliance in normotensive and hypertensive rats. *J. CV Pharmacol.* **7**, S28–S32.

Liu, S. Q. & Fung, Y. C. 1988 Zero-stress state of arteries. *J. Biomech. Eng.* **110**, 82–84.

Liu, S. Q. & Fung, Y. C. 1989 Relationship between hypertension, hypertrophy, and opening angle of zero-stress state of arteries following aortic constriction. *ASME J. Biomech. Eng.* **111**, 325–335.

Liu, S. Q. & Fung, Y. C. 1992 Changes of rheological properties of the blood vessels due to tissue remodeling in the course of development of diabetes. *Biorheology* **29**, 443–457.

Liu, S. Q. & Fung, Y. C. 1993 Changes in the structure and mechanical properties of pulmonary arteries of rats exposed to cigarette smoke. *Am. Rev. Respir. Dis.* **148**, 768–777.

Long, A., Rouet, L., Bissery, A., Goeau-Brissonniere, O. & Sapoval, M. 2004 Aortic compliance in healthy subjects: evaluation of tissue Doppler imaging. *Ultrasound Med. Biol.* **30**, 753–779. (doi:10.1016/j.ultrasmedbio.2004.03.007)

Lu, X., Zhao, J. B., Wang, G. R., Gregersen, H. & Kassab, G. S. 2001 Remodeling of the zero-stress state of the femoral artery in response to flow-overload. *Am. J. Physiol. Heart Circ. Physiol.* **280**, H1547–H1559.

Marchii, M. & Becker, A. E. 1997 Morphologic features of the normal aortic arch in neonates, infants, and children pertinent to growth. *Ann. Thorac. Surg.* **64**, 511–515. (doi:10.1016/S0003-4975(97)00445-1)

Marquardt, D. W. 1963 An algorithm for least-squares estimation of nonlinear parameters. *J. Soc. Ind. Appl. Math.* **2**, 431–441. (doi:10.1137/0111030)

Matsumoto, T. & Hayashi, K. 1994*a* Mechanical and dimensional adaptation of rat aorta to hypertension. *J. Biomech. Eng.* **116**, 278–283.

Matsumoto, T. & Hayashi, K. 1994*b* Mechanical and dimensional adaptation of rat aorta to hypertension. *Tans. ASME, J. Biomech. Eng* **116**, 278–283.

McDonald, D. A. 1974 *Blood flow in arteries*. Baltimore, MD: William Wilkins.

McGuigan, E. A., Sears, S. T., Corse, W. R. & Ho, V. B. 2005 MR angiography of the abdominal aorta. *Magn. Reson. Imaging Clin. N. Am.* **13**, 65–89. (doi:10.1016/j.mric.2004.12.010)

Murase, K., Naruse, K., Kimura, A., Okumura, K., Hayakawa, T. & Sokabe, M. 2001 Protamine auguments stretch induced calcium increase in vascular endothelium. *Br. J. Pharmacol.* **134**, 1403–110. (doi:10.1038/sj.bjp.0704386)

Naruse, K. & Sokabe, M. 1993 Involvement of stretch-activated ion channels in Ca2+ mobilization to mechanical stretch in endothelial cells. *Am. J. Physiol.* **264**(4 Pt 1), C1037–C144.

Naruse, K., Sai, X., Yokoyama, N. & Sokabe, M. 1998 Uniaxial cyclic stretch induces c-src activatin and translocation in human endothelial cells via SA channel activation. *Febs. Lett.* **441**, 111–115. (doi:10.1016/S0014-5793(98)01528-2)

Nayfeh, A. H. & Kress, G. R. 1997 Non-linear constitutive model for plain-weave composites. *Compos. Part B-Eng.* **28**, 627–634. (doi:10.1016/S1359-8368(96)00079-0)

Nichols, W. M. & O'Rourke, M. F. 1990 *McDonald's blood flow in arteries: theoretical, experimental and clinical principles*, 3rd edn. Philadelphia, PA: Lea and Febiger Publishing.

Oka, S. 1972 Some theoretical studies on hemorheology. In *Advances in biophysics*, vol. 3 (ed. M. Kotani), p. 97. Tokyo, Japan: Univesity of Tokyo Press.

Oka, S. & Azuma, T. 1970 Physical theory of tension in thick walled blood vessels in equilibrium. *Biorheology* **7**, 109.

Olivetti, G., Anversa, P., Melissari, M. & Loud, A. V. 1980 Morphometric study of early postnatal development of the thoracic aorta in the rat. *Circ. Res.* **47**, 417–424.

O'Rourke, M. 1994 Arterial stiffening and vascular/ventricular interaction. *J. Hum. Hypertens.* **8**(Suppl. 1), S9–S15.

O'Rourke, M. F. & Nichols, W. W. 2005 Aortic diameter, aortic stiffness, and wave reflection increase with age and isolated systolic hypertension. *Hypertension* **45**, 652–668. (doi:10.1161/01.HYP.0000153793.84859.b8)

Pandit, A., Lu, X & Kassab, G. S. 2005 The biaxial elastic material properties of porcine coronary media and adventitia. *Am. J. Physiol. Heart Circ. Physiol.* **288**, H2581–H2587. (doi:10.1152/ajpheart.00648.2004)

Patel, D. J. & Fry, D. L. 1966 Longitudinal tethering of arteries in dogs. *Circ. Res.* **19**, 1011–1021.

Patel, D. J. & Vaishnav, R. N. 1972 The rheology of large blood vessels. In *CV Fluid dynamics*, vol. 2 (ed. D. H. Berge), pp. 1–64. New York, NY: Academic Press.

Patel, D. J., Janicki, J. S., Vaishnav, R. N. & Young, J. T. 1973 Dynamic anisotropic viscoelastic properties of the aorta in living dogs. *Circ. Res.* **32**, 93–107.

Plump, A. S., Smith, J. D., Hayek, T., Aalto-Setala, K., Walsh, A., Verstuyft, J. G., Rubin, E. M. & Breslow, J. L. 1992 Severe hypercholesterolemia and atherosclerosis in apolipoprotein E-deficient mice created by homologous recombination in ES cells. *Cell* **71**, 343. (doi:10.1016/0092-8674(92)90362-G)

Rachev, A. & Greenwald, S. E. 2003 Residual strains in conduit arteries. *J. Biomech.* **36**, 661–670. (doi:10.1016/S0021-9290(02)00444-X)

Rachev, A., Stergiopulos, N. & Meister, J. J. 1996 Theoretical study of dynamics of arterial wall remodeling in response to changes in blood pressure. *J. Biomech.* **29**, 635–642. (doi:10.1016/0021-9290(95)00108-5)

Rhodin, J. A. G. 1979 Architecture of the vessel wall. In *Handbook of physiology* (ed. R. M. Berne) *Section 2: the cardiovascular system*, vol. 2. Bethesda, MD: American Physiology Society.

Roach, M. R. & Burton, A. C. 1959 The effect of age on the elasticity of human iliac arteries. *Can. J. Biochem. Physiol.* **37**, 557–570.

Rubinstein, M. & Panyukov, S. 2002 Elastic of polymer networks. *Macromolecules* **35**, 6670–6686. (doi:10.1021/ma0203849)

Russell, E. S. 1966 Lifespan and aging patterns. In *The biology of the laboratory mouse* (ed. E. L. Green) pp. 511–519, 2nd edn. New York, NY: Dover.

Russell, E. S. 1972 Genetic considerations in the selection of rodent species and strains for research in aging. In *Development of the rodent as a model system of aging* (ed. D. Gibson), pp. 33–35. Bethesda, MD: DHEW, Pub No (NIH) 72–121.

Russell, E. S. & Meier, H. 1966 Constitutional diseases. In *The biology of the laboratory mouse* (ed. E. L. Green) pp. 571–587, 2nd edn. New York, NY: Dover.

Sachs, F. 1988 Mechanical transduction in biological systems. *CRC Crit. Rev. Biomed. Eng.* **16**, 141–169.

Sack, W. O. 1982 *Essentials of pig anatomy*. Ithaca, NY: Veterinary Textbooks.

Safar, M. E., London, G. M., Asmar, R. & Frohlich, E. D. 1998 Recent advances on large arteries in hypertension. *Hypertension* **32**, 156–161.

Saini, A., Berry, C. & Greenwald, S. 1995 Effect of age and sex on residual stress in the aorta. *J. Vasc. Res.* **32**, 398–405.

Salomma, V., Riley, W., Kark, J. D., Nardo, C. & Folsom, A. R. 1995 Non-insulin-dependent diabetes mellitus and fasting glucose and insulin concentrations are associated with arterial stiffness indexes. The ARIC study. Atherosclerosis Risk in Communites Study. *Circulation* **91**, 1432–1443.

Silver, F. H., Christiansen, D. L. & Buntin, C. M. 1989 Mechanical properties of the aorta: a review. *Crit. Rev. Biomed. Eng.* **17**, 323–358.

Singer, C. 1959 *A short history of scientific ideas to 1900*. New York, NY: Oxford University Press.

Slordahl, S. A., Piene, H, Solbakken, J. E., Rossvoll, O., Samstad, S. O. & Angelsen, B. A. J. 1990 Estimation of arterial compliance in aortic regurgitation: three methods evaluated in pigs. *Med. Bio. Eng. Comput.* **28**, 293–299.

Sobin, S. S. & Chen, P. C. Y. 1997 Vascular cylindricity in animals and plants. *Ann. Biomed. Eng.* **25**, S-S32.

Stefanadis, C., Tsinmis, E., Vlachopoulos, C., Stratos, C., Toutouzas, K., Pitsavos, C., Marakas, S., Boudoulas, H. & Toutouzas, P. 1997 Unfavorable effect of smoking on the elastic properties of the human aorta. *Circulation* **95**, 31–38.

Stergioulos, N., Segers, P. & Westerhof, N. 1999 Use of pulse pressure method for estimating total arterial compliance *in vivo*. *Am. J. Physiol. Heart Circ. Physiol.* **276**, H424–H428.

Storer, J. B. 1966 Longevity and gross pathology at death in 22 inbreed mouse strains. *J. Gerontol.* **21**, 404–409.

Sucov, H. M. 1998 Molecular insights into cardiac development. *Annu. Rev. Physiol.* **60**, 287–308. (doi:10.1146/annurev.physiol.60.1.287)

Sverdlik, A. & Lanir, Y. 2002 Time-dependent mechanical behavior of sheep digital tendons, including the effects of preconditioning. *J. Biomech. Eng.* **124**, 78–84. (doi:10.1115/1.1427699)

Taber, L. A. & Humphrey, J. D. 2001 Stress-modulated growth, residual stress, and vascular heterogeneity. *J. Biomech. Eng. Trans. ASME* **123**, 528–535. (doi:10.1115/1.1412451)

Takamizawa, K. & Hayashi, K. 1987 Strain-energy density-function and uniform strain hypothesis for arterial mechanics. *J. Biomech.* **20**, 7–17. (doi:10.1016/0021-9290(87)90262-4)

Takamizawa, K. & Hayashi, K. 1988 Uniform strain hypothesis and thin-walled theory in arterial mechanics. *Biorheology* **25**, 555–565.

Tanaka, T. T. & Fung, Y. C. 1974 Elastic and inelastic properties of the canine aorta and their variation along the aortic tree. *J. Biomech.* **7**, 357–370. (doi:10.1016/0021-9290(74)90031-1)

Thompson, B. H. & Stanford, W. 1994 Electron beam computed tomographic imaging of aortic aneurysms and dissections. *J. Invasive Cardiol.* **6**, 213–227.

Treloar, L. R. G. 1975 *The physics of rubber elasticity*. Oxford, UK: Clarendon Press.

Tseng, H., Peterson, T. E. & Berk, B. C. 1995 Fluid shear stress stimulates mitogen-activated protein kinase in endothelial cells. *Circ. Res.* **77**, 869–878.

Vaishnav, R. N. & Vossoughi, J. 1983 Estimation of residual strains in aortic segments. In *Biomedical engineering II, recent developments*, vol. 2 (ed. C. W. Hall), pp. 330–333. New York, NY: Pergamon Press.

Vaishnav, R. N., Vossoughi, J., Patel, D. J., Cothran, L. N., Coleman, B. R. & Ison-Franklin, E. L. 1990 Effect of hypertension on elasticity and geometry of aortic tissue from dogs. *J. Biomech. Eng.* **112**, 70–74.

Vigdergauz, S. 2001 The effective properties of a performated elastic plate: numerical optimization by genetic algorithm. *Int. J. Solids Struct.* **38**, 8593–8616. (doi:10.1016/S0020-7683(01)00189-5)

Vito, R. P. & Dixon, S. A. 2003 Blood vessel constitutive models-1995–2002. *Annu. Rev. Biomed. Eng.* **5**, 413–439. (doi:10.1146/annurev.bioeng.5.011303.120719)

Weizsacker, H. W., Lambert, H. & Pascale, K. 1983 Analysis of the passive mechanical properties of rat carotid arteries. *J. Biomech.* **16**, 703–715. (doi:10.1016/0021-9290(83)90080-5)

Wells, S. M., Langille, B. L. & Adamson, S. L. 1998 *In vivo* and *in vitro* mechanical properties of the sheep thoracic aorta in the perinatal period and adulthood. *Am. J. Physiol. Heart Circ. Physiol.* **274**, H1749–H1760.

White, F. C. & Bloor, C. M. 1981 Coronary collateral circulation in the pig: correlation of collateral flow with coronary bed size. *Basic Res. Cardiol.* **76**, 189–196. (doi:10.1007/BF01907957)

Wiesmann, F., Ruff, J., Hiller, K. H., Rommel, E., Haase, A. & Neubauer, S. 2000 Developmental changes of cardiac function and mass assessed with MRI in neonatal, juvenile, and adult mice. *Am. J. Physiol. Heart Circ. Physiol.* **278**, H652–H657.

Wolinsky, H. 1971 Effects of hypertension and its reversal on the thoracic aorta of male and female rats. *Circ. Res.* **28**, 622–637.

Wolinsky, H. 1972 Long-term effects of hypertension o the rat aortic wall and their relation to concurrent aging changes. *Circ. Res.* **30**, 301–309.

Wolinsky, H. & Glagov, S. 1967 A lamellar unit of aortic medial structure and function in mammals. *Circ. Res.* **20**, 99–111.

Wong, L. C. Y. & Langille, B. L. 1996 Developmental remodeling of the internal elastic lamina of rabbit arteries—effect of blood flow. *Circ. Res.* **78**, 799–805.

Young, J. 1930 Malpighi's "de Pulmonibus.". *Proc. R. Soc. Med.* **23**, 1–14.

Zarins, C. K., Zatina, M. A., Giddens, D. P., Ku, D. N. & Glagov, S. 1987 Shear stress regulation of artery lumen diameter in experimental atherogenesis. *J. Vasc. Surg.* **5**, 413–420. (doi:10.1067/mva.1987.avs0050413)

Zhang, W., Herrera, C., Atluri, S. N. & Kassab, G. S. 2004 The effect of surrounding tissue on vessel fluid and solid mechanics. *J. Biomech. Eng.* **126**, 760–769. (doi:10.1115/1.1824128)

Zhang, W., Herrera, C., Atluri, S. N. & Kassab, G. S. 2005 The effect of longitudinal pre-stretch and radial constraint on the stress distribution in the vessel wall: a new hypothesis. *Mech. Chem. Biosystems* **2**, 41–52.

Zoumi, A., Yeh, A. & Tromberg, B. J. 2002 Imaging cells and extracellular matrix *in vivo* by using second-harmonic generation and two-photon excited fluorescence. *Proc. Natl Acad. Sci. USA* **99**, 11 014–11 019. (doi:10.1073/pnas.172368799)

Zoumi, A., Lu, X., Kassab, G. S. & Tromberg, B. J. 2004 Selective imaging of coronary artery micro-structural components using multi-photon microscopy. *Biophys. J.* **87**, 2778–2286. (doi:10.1529/biophysj.104.042887)